INSTITUTE FOR FUSION STUDIES

DOE/ET-53088-537 IFSR #537

Mode Structure and Continuum Damping of High-n Toroidal Alfvén Eigenmodes

M.N. ROSENBLUTH
Department of Physics
University of California, San Diego
La Jolla, CA 92093
and
H.L. BERK, J.W. VAN DAM, D.M. LINDBERG
Institute for Fusion Studies
The University of Texas at Austin
Austin, Texas 78712

February 1992

THE UNIVERSITY OF TEXAS

AUSTIN

Mode Structure and Continuum Damping of High-n Toroidal Alfvén Eigenmodes

M.N. Rosenbluth
Department of Physics
University of California, San Diego
La Jolla, CA 92093
and
H.L. Berk, J.W. Van Dam, D.M. Lindberg
Institute for Fusion Studies
The University of Texas at Austin
Austin, Texas 78712

Abstract

An asymptotic theory is described for calculating the mode structure and continuum damping of short-wavelength toroidal Alfvén eigenmodes (TAE). The formalism somewhat resembles the treatment used for describing low-frequency toroidal modes with singular structure at a rational surface, where an inner solution, which for the TAE mode has toroidal coupling, is matched to an outer toroidally uncoupled solution. A three-term recursion relation among coupled poloidal harmonic amplitudes is obtained, whose solution gives the structure of the global wavefunction and the complex eigenfrequency, including continuum damping. Both analytic and numerical solutions are presented. The magnitude of the damping is essential for determining the thresholds for instability driven by the spatial gradients of energetic particles (e.g., neutral beam-injected ions or fusion-product alpha particles) contained in a tokamak plasma.

I. Introduction

In a burning plasma, significant numbers of highly energetic alpha particles will be produced, which can interact with the core plasma and affect its stability and confinement. Of particular interest are shear Alfvén waves, since the alpha particles in a deuterium-tritium plasma are born at an energy of 3.5 MeV, which corresponds to a speed higher than the Alfvén speed for typical reactor parameters. It was earlier shown[1,2] that circulating alpha particles can destabilize shear Alfvén waves through wave-particle interaction at the resonance $\omega = k_{\|} v_{\|\alpha}$. These shear Alfvén waves normally experience significant Landau damping, due to their short radial wavelengths. However, an exception occurs with the so-called toroidal Alfvén eigenmode (TAE), which is a discrete shear Alfvén wave whose frequency lies within "gaps" in the frequency spectrum that are induced by toroidicity.[3,4] The TAE mode can be strongly excited by alpha particles.[5–7] Furthermore, the presence of this unstable wave can cause rapid anomalous loss of confined alpha particles.[8] Two recent experiments have indicated that parallel neutral injection of sufficiently fast ions can trigger the TAE mode.[9,10] The quasilinear saturation of a single mode of this instability has also been studied.[11]

Since the stability of the TAE mode is relevant not only to burning plasma experiments, but also to applications that will use high-power neutral beam injection for heating or current drive, it has become the subject of considerable attention. In order to be able to predict the threshold, an accurate calculation of the damping is necessary. Early studies of TAE stability focused on collisionless Landau damping.[5,6,12–18] It was then pointed out that for the low-mode-number TAE modes, Alfvén continuum damping could be significant.[19] Also, collisional Landau damping between trapped and passing electrons has been estimated.[20]

In the present paper, we give a detailed description of a general asymptotic theory for calculating the continuum damping rate for high-mode-number TAE modes.[21] The theory

assumes low beta, large aspect ratio, and circular cross section. The results indicate that continuum damping can be significant, even comparable to alpha-particle induced growth rates, as long as the shear is not too small or the mode number too large. (Estimates of the TAE growth rate due to fast ion or alpha particle resonance are given, for example, in Refs. 5, 6, and 14-19.)

Another analytic calculation of the high-mode-number TAE continuum damping rate has been carried out recently,[22] with the use of the "ballooning" representation, in the low shear limit. These results resemble ours, although the scaling of the damping rate with mode number reported in Ref. 22 is different. Our analytic results are supported by numerical calculations.

Two computational studies, one with an initial value code[23] and the other with a resistive eigenvalue code,[24] have recently obtained continuum damping rates for low-mode-number TAE modes comparable to those calculated herein.

In Sec. II of the present paper, the toroidally coupled eigenmode equations are derived, and a brief description of the physics of TAE modes is presented. Analytic solutions of the finite difference eigenmode equation in various limits are obtained and compared to numerical solutions in Sec. III; also, the theory is extended to allow for broad profiles. Discussion and concluding comments are given in Sec. IV. An appendix describes the details of the theoretical derivation for the eigenmode structure.

II. Eigenmode Equations

We consider a low-beta plasma ($\beta \equiv 8\pi p/B^2 \ll 1$) in a large-aspect-ratio tokamak ($a/R \ll 1$) with circular cross-section. Furthermore, we will consider waves with large mode numbers, so that radial derivatives of the perturbed wavefunction dominate over poloidal derivatives.

In ideal MHD theory, the vanishing of the parallel perturbed electric field gives a rela-

tionship between the electrostatic potential ϕ and the vector potential $A_{||}$:

$$-\,\mathbf{b}\cdot\nabla\phi + i\omega A_{||} = 0\ , \qquad \text{with} \quad \mathbf{b} = \frac{\mathbf{B}}{B_0}\ . \tag{1}$$

Charge neutrality is expressed by the current being divergence-free:

$$\mathbf{b}\cdot\nabla J_{||} + \nabla\cdot\left(\frac{\mathbf{B}\times\rho\,\frac{\partial\mathbf{v}}{\partial t}}{B^2}\right) = 0\ . \tag{2}$$

The parallel perturbed current is given by Ampére's law,

$$4\pi\, J_{||} = -\nabla^2\, A_{||}\ , \tag{3}$$

with the fluid velocity given by $\mathbf{E}\times\mathbf{B}$ motion,

$$\mathbf{v} = -\frac{\nabla\phi\times\mathbf{B}}{B^2}\ . \tag{4}$$

By combining Eqs. (1)–(4), we obtain the reduced-MHD equation for high-mode-number shear Alfvén waves:

$$(\mathbf{b}\cdot\nabla)\left[\nabla^2(\mathbf{b}\cdot\nabla)\phi\right] + \nabla\cdot\left(\frac{\omega^2}{v_A^2}\,\nabla\phi\right) = 0\ . \tag{5}$$

Here, $v_A = B/(4\pi\rho)^{1/2}$ is the Alfvén speed, with B the magnitude of the magnetic field and ρ the mass density (mostly that of the plasma ions). By virtue of periodicity in the poloidal θ-direction and in the toroidal ζ-direction in a tokamak plasma, a wave field perturbation with frequency ω can be described by a Fourier decomposition in poloidal harmonics as $\phi(r,\theta,\zeta,t) = \sum_m \phi_m(r)\exp[-im\theta + in\zeta - i\omega t]$, where n is a "good" quantum number due to toroidal symmetry. Then we have $(\mathbf{b}\cdot\nabla)\phi \to ik_{||m}\,\phi_m$, where the parallel wavenumber for the mth harmonic is given by

$$k_{||m}(r) = \frac{1}{R}\left(n - \frac{m}{q(r)}\right)\ , \tag{6}$$

with r and R the minor and major radii, respectively, and $q(r) = rB_\zeta/RB_\theta$ the safety factor.

In toroidal geometry, however, the equilibrium quantities are functions of θ: e.g., the magnetic field strength is $B \cong B_0[1-(r/R)\cos\theta]$. This leads to coupling among the poloidal

harmonics. To lowest order in the basic expansion parameter $r/R \ll 1$, ϕ_m couples only to its neighboring sidebands, $\phi_{m\pm1}$, and Eq. (5) reduces to a system of coupled equations given by

$$\frac{d}{dr}\left[\left(\frac{\omega^2}{v_A^2} - k_{\|m}^2\right)\frac{d\phi_m}{dr}\right] - \frac{m^2}{r^2}\left(\frac{\omega^2}{v_A^2} - k_{\|m}^2\right)\phi_m + \varepsilon\frac{\omega^2}{v_A^2}\left(\frac{d^2\phi_{m-1}}{dr^2} + \frac{d^2\phi_{m+1}}{dr^2}\right) = 0 \ . \quad (7)$$

where $k_{\|m}r \ll 1$ and $m \gg 1$ have been used. In Eq. (7), $\varepsilon(r) \ll 1$ is the toroidicity coupling strength; elsewhere[19] it is shown that $\varepsilon \cong 5r/2R$ for a low-beta tokamak plasma.

In the $\varepsilon \to 0$ limit, the poloidal harmonics $\phi_m(r)$ are uncoupled, and Eq. (7) exhibits singular structure at points $r = r_s$ where the coefficient of the second derivative term vanishes. For a real frequency ω, this leads to the shear Alfvén wave resonance condition,

$$\omega = k_{\|m}(r_s)\, v_A(r_s) \ . \quad (8)$$

It can be shown from ideal MHD theory that, as a consequence of causality, if an external excitation is applied at a real frequency ω, absorption of energy by the plasma will occur at the point r_s, which is the manifestation of continuum mode damping.

By the same argument, at special degenerate frequencies (the so-called TAE frequencies), it will appear that absorption from two wave harmonics with neighboring mode numbers occurs at the same spatial location. Specifically, at the points $r = r_m$ where $k_{\|m-1}(r_m) = -k_{\|m}(r_m) = 1/(2q_mR)$, with $q_m = q(r_m) = (m - 1/2)/n$, an excitation applied at the degenerate frequency $\omega = v_A(r_m)/2q_mR$ will lead to apparent energy absorption by the plasma at $r = r_m$ from both the $m - 1$ and m harmonics of the wave. If, however, ε is small but nonzero, the degeneracy at the TAE frequencies will be resolved by coupling of the harmonics through the toroidicity, which will cause spectral "gaps" of width $\approx \varepsilon$ to be formed in the Alfvén continuum. This allows local energy absorption to be avoided. With nonzero ε, the precise condition for the singular structure in Eq. (7) is the vanishing of the determinant whose elements are the coefficients of the terms with the highest derivatives

of the ϕ_m. A radial plot of these singular frequencies, which comprise the toroidal shear Alfvén continuum, is shown in Fig. 1 for a typical equilibrium — viz., constant density and $q(r) = q(0) + [q(a) - q(0)](r/a)^2$ with $q(0) = 1.0$ and $q(a) = 2.5$ — and for various poloidal mode numbers m, with $n = 5$ and $a/R = 0.25$. The gap structure in the continuum of singular frequencies is induced by the toroidal coupling, which prevents the resonant frequencies from being crossed. Thus, it is possible for an externally applied frequency to thread through several gaps, while avoiding the dissipative Alfvén resonance that would have occured in the cylindrical $\varepsilon = 0$ limit. In general, some resonances cannot be avoided, and they need to be calculated in the toroidal limit.

With toroidicity, the shear Alfvén gap structure also allows for natural modes of oscillation, the discrete toroidal Alfvén eigenmodes, to exist within the gaps, with eigenfrequencies ω that are near the TAE frequencies. However, a TAE mode may still be damped, since it can interact dissipatively with the continuum in regions that are somewhat remote from the region where the mode is principally localized. In the present paper, we will determine the mode structure and the magnitude of the instrinsic continuum damping for the TAE modes.

To develop our theory, we search for an eigenfrequency ω that is near a specific TAE frequency $\omega_{\rm TAE}(r_{m_0}) = v_A(r_{m_0})/2q(r_{m_0})R$ associated with the interaction of the m_0 and $m_0 - 1$ harmonics at the point $r = r_{m_0}$, where $q(r_{m_0}) = (m_0 - \frac{1}{2})/n$. The eigenfrequency, ω, is expressed in terms of a complex mismatch parameter, g_0, defined through

$$\omega^2 = \frac{\omega^2_{\rm TAE}(r_{m_0})}{1 - \epsilon_0\, g_0}\ , \tag{9}$$

with $\epsilon_0 = \epsilon(r_{m_0})$. We also introduce the complex mismatch parameter, g_ℓ, associated with the shift of the eigenfrequency from the $m_0+\ell$ TAE frequency (for arbitrary sideband number ℓ), defined by

$$\omega^2 = \frac{\omega^2_{\rm TAE}(r_{m_0+\ell})}{1 - \epsilon_\ell\, g_\ell} \tag{10}$$

with $\epsilon_\ell = \epsilon(r_{m_0+\ell})$ and $\omega_{\rm TAE}(r_{m_0+\ell}) = v_A(r_{m_0+\ell})/2q(r_{m_0+\ell})R$ the TAE frequency associated

with the interaction of the $m_0+\ell$ and $m_0+\ell-1$ harmonics at $r=r_{m_0+\ell}$, where $q(r_{m_0+\ell})=\left(m_0+\ell-\frac{1}{2}\right)/n$. Note that

$$\frac{1-\epsilon_0 g_0}{1-\epsilon_\ell g_\ell}=\frac{v_A^2(r_0)q_\ell^2}{v_A^2(r_\ell)q_0^2}=1+(q_\ell-q_0)\left[\frac{\partial}{\partial q}\ln\left(\frac{q^2}{v_A^2}\right)\right]_{r=r_0}+\cdots\,, \tag{11}$$

where we have suppressed the dependence on m_0 so that $r_\ell=r_{m_0+\ell}$ and $q_\ell=q(r_{m_0+\ell})$, and where we will denote $\phi_{m_0+\ell}$ as ϕ_ℓ. Therefore, if $\ell\ll m_0$ and in the limit $\epsilon_\ell\, g_\ell\ll 1$, we can approximate the exact relation between g_ℓ and g_0 by the first order expansion

$$g_\ell\cong g_0+\frac{2\ell}{m_0\widehat{\epsilon}} \tag{12}$$

with $\widehat{\epsilon}=\epsilon_0\left[\partial\ln(q^2/v_A^2)/\partial\ln q^2\right]^{-1}_{q=q_0}$.

In analyzing Eq. (7) we assume toroidal coupling is significant only near the TAE locations. Expanding Eq. (7) about the location $r=r_\ell$ where only the interaction between the ℓ and $\ell-1$ harmonics is significant and introducing the variable $x=n\left[q(r)-\frac{m_0}{n}\right]\cong nq'(r_\ell)(r-r_\ell)-1/2$, we obtain the following coupled equations (for general $\epsilon_\ell\, g_\ell$):

$$\frac{d}{dx}\left[\frac{1}{4(1-\epsilon_\ell g_\ell)}-(x-\ell)^2\right]\frac{d\phi_\ell}{dx}-\frac{1}{S_\ell^2}\left[\frac{1}{4(1-\epsilon_\ell g_\ell)}-(x-\ell)^2\right]\phi_\ell \tag{13}$$

$$+\frac{\epsilon_\ell}{4(1-\epsilon_\ell g_\ell)}\frac{d^2\phi_{\ell-1}}{dx^2}=0\,,$$

$$\frac{d}{dx}\left[\frac{1}{4(1-\epsilon_\ell g_\ell)}-(x-\ell+1)^2\right]\frac{d\phi_{\ell-1}}{dx}-\frac{1}{S_\ell^2}\left[\frac{1}{4(1-\epsilon_\ell g_\ell)}-(x-\ell+1)^2\right]\phi_{\ell-1}+\frac{\epsilon_\ell}{4(1-\epsilon_\ell g_\ell)}\frac{d^2\phi_\ell}{dx^2}=0 \tag{14}$$

where terms that are $\mathcal{O}(1/n)$ or $\mathcal{O}(\epsilon)$ have been neglected. Here, $S_\ell=[d(\ln q)/d(\ln r)]_{r=r_\ell}$ is the value of the shear at the ℓth gap location. The coupling of the ℓ harmonic with the $\ell+1$ harmonic near $r=r_{\ell+1}$, where $q=(m_0+\ell+\frac{1}{2})/n\equiv q_{\ell+1}$ is also governed by Eqs. (13) and (14) with $\ell\to\ell+1$.

It is now clear that for $|x-\ell\mp 1/2|\gg\epsilon$, the equation for ϕ_ℓ is nearly independent of toroidal coupling and is given by

$$\frac{d}{dx}\left[\frac{1}{4}-(x-\ell)^2\right]\frac{d\phi_\ell}{dx}-\frac{1}{S_\ell^2}\left[\frac{1}{4}-(x-\ell)^2\right]\phi_\ell=0\,, \tag{15}$$

where the difference between S_ℓ and $S_{\ell+1}$ is small and ignorable. However, within the narrow layers where $|x - \ell \mp 1/2| \lesssim \epsilon$, the toroidal coupling must be taken into account. In these regions, the terms containing second-order derivatives dominate because of the nearly singular structure of the equation for small ϵ. Thus, near such a singular layer (say, $x - \ell \approx -1/2$), Eqs. (13) and (14) reduce to

$$\frac{d}{dx}\left\{\left[\frac{\epsilon_\ell\, g_\ell}{4(1-\epsilon_\ell\, g_\ell)} + x - \ell + 1/2\right]\frac{d\phi_\ell}{dx} + \frac{\epsilon_\ell}{4(1-\epsilon_\ell g_\ell)}\frac{d\phi_{\ell-1}}{dx}\right\} \cong 0 \tag{16}$$

$$\frac{d}{dx}\left\{\left[\frac{\epsilon_\ell\, g_\ell}{4(1-\epsilon_\ell\, g_\ell)} - (x - \ell + 1/2)\right]\frac{d\phi_{\ell-1}}{dx} + \frac{\epsilon_\ell}{4(1-\epsilon_\ell g_\ell)}\frac{d\phi_\ell}{dx}\right\} \cong 0\,. \tag{17}$$

This leads to a boundary value problem, with the solution of Eq. (15) to be matched to the toroidally coupled solution of Eqs. (16) and (17).

A. Solution away from a gap

Outside the thin layer at each gap within which toroidal coupling occurs, the harmonics, $\phi_\ell(x)$, are essentially uncoupled and satisfy Eq. (15).

Consider the properties of the solution to Eq. (15). At large $|x - \ell|$, the solution behaves as either a growing or decaying exponential; for well-behavedness we require a decaying solution:

$$\phi_\ell(x_\ell) \to \frac{1}{x_\ell}\exp\left(-\frac{|x_\ell|}{S_\ell}\right)\,, \qquad \text{for} \quad |x_\ell| \gg \frac{1}{2S_\ell}\,, \tag{18}$$

with $x_\ell \equiv x - \ell$. Near the TAE points $x_\ell = \pm 1/2$, the solution has the form

$$\phi_\ell(x_\ell) \to C_\ell^{L,R}\left[\ln\left|x_\ell^2 - \frac{1}{4}\right| + \Delta_\ell\right]\,, \qquad \text{for} \quad x_\ell \to \pm\frac{1}{2}\,. \tag{19}$$

In Eq. (19), the constants $C_\ell^L = C_\ell(x_\ell = -1/2)$ and $C_\ell^R = C_\ell(x_\ell = 1/2)$ are the coefficients of the logarithmically divergent part of the solution at the "left" and "right" gaps, and Δ_ℓ is proportional to the constant regular part of the solution. Finally, with respect to the point $x_\ell = 0$, the solution for $\phi_\ell(x_\ell)$ is, in general, a superposition of symmetric and antisymmetric solutions.

Three particular values for Δ_ℓ characterize the general solution. First, consider the solution in the regions where $|x_\ell| > 1/2$: we define Δ_∞ as the value of Δ corresponding to the solution that is well behaved as $|x_\ell| \to \infty$, i.e., has the behavior given in Eq. (18). Next, consider the solution in the region $|x_\ell| < 1/2$ between the two gaps: if $\Delta = \Delta_s$, the solution is symmetric with respect to $x_\ell = 0$ (i.e., has the property that $C_\ell^L = C_\ell^R$); and if $\Delta = \Delta_a$, the solution is antisymmetric (i.e., $C_\ell^L = -C_\ell^R$). These three particular values of Δ can be tabulated as functions of S_ℓ only. The functional forms for $\Delta_\infty(S)$, $\Delta_s(S)$, and $\Delta_a(S)$ can be derived analytically in the limits of small and large shear and are given in Table I.

B. Matching to the solution near the gaps

In the narrow layers near the gaps, the harmonics ϕ_ℓ obey Eqs. (13) and (14). Consider the gap at $x_\ell = -1/2$. The first integrals of the two coupled equations (16) and (17) can immediately be written down:

$$\left(\frac{1}{2} + x_\ell + \frac{\varepsilon'_\ell\, g_\ell}{4}\right)\frac{d\phi_\ell}{dx_\ell} + \frac{\varepsilon'_\ell}{4}\frac{d\phi_{\ell-1}}{dx_\ell} = C_\ell^L \tag{20}$$

$$\left(\frac{1}{2} + x_\ell - \frac{\varepsilon'_\ell\, g_\ell}{4}\right)\frac{d\phi_{\ell-1}}{dx_\ell} - \frac{\varepsilon'_\ell}{4}\frac{d\phi_\ell}{dx_\ell} = C_{\ell-1}^R \tag{21}$$

where $\varepsilon'_\ell = \varepsilon_\ell/(1-\varepsilon_\ell\, g_\ell)$ and where the constants on the right-hand sides of Eqs. (20) and (21) are found by asymptotically matching to the solution away from the gap for $|x_\ell+1/2|/\varepsilon \gg 1$. Now invert Eqs. (20) and (21):

$$\frac{d\phi_\ell}{dx} = \frac{\left(\frac{1}{2} + x_\ell - \frac{\varepsilon'_\ell}{4}\, g_\ell\right) C_\ell^L - \frac{\varepsilon'_\ell}{4}\, C_{\ell-1}^R}{\left(\frac{1}{2} + x_\ell\right)^2 + \left(\frac{\varepsilon'_\ell}{4}\right)^2 (1 - g_\ell^2)}\,, \tag{22}$$

$$\frac{d\phi_{\ell-1}}{dx} = \frac{\frac{\varepsilon'_\ell}{4}\, C_\ell^L + \left(\frac{1}{2} + x_\ell + \frac{\varepsilon'_\ell\, g_\ell}{4}\right) C_{\ell-1}^R}{\left(\frac{1}{2} + x_\ell\right)^2 + \left(\frac{\varepsilon'_\ell}{4}\right)^2 (1 - g_\ell^2)}\,. \tag{23}$$

By integrating Eqs. (22) and (23), we obtain the jump conditions for the changes in the magnitude of the harmonics across the gap region:

$$J_\ell^L \equiv \lim_{\delta/\varepsilon\to\infty} \int_{-1/2-\delta}^{-1/2+\delta} dx_\ell \left(\frac{d\phi_\ell}{dx_\ell}\right) = \pi\left(\alpha_\ell\, C_\ell^L + \beta_\ell\, C_{\ell-1}^R\right) \tag{24}$$

and

$$J^R_{\ell-1} = -\pi \left(\alpha_\ell \, C^R_{\ell-1} + \beta_\ell \, C^L_\ell \right) \ , \tag{25}$$

with

$$\alpha_\ell = -\frac{g_\ell}{\sqrt{1-g_\ell^2}} \ , \qquad \beta_\ell = -\frac{1}{\sqrt{1-g_\ell^2}} \ . \tag{26}$$

If we consider the gap at $x_\ell = 1/2$, we obtain the same set of jump conditions as when we let $\ell \to \ell + 1$ in Eqs. (24) and (25).

For g_ℓ^2 real, the branch of the square root $(1-g_\ell^2)^{1/2}$ needs to be defined. In the case when $\mathrm{Re}(g_\ell^2) < 1$, we take the square root to be positive. In the case when $\mathrm{Re}(g_\ell^2) > 1$, causality arguments determine the proper analytic continuation. This is done by formally adding an infinitesimal imaginary part to the frequency that is positive (consistent with causality), to determine whether to slightly deform the x_ℓ integral up or down into the complex x_ℓ-plane, in order to go around the singularities at $(x_\ell + 1/2)^2 = (\varepsilon/4)^2 (g_\ell^2 - 1)^{1/2}$. In this way we obtain the following prescription for real g_ℓ:

$$\sqrt{1-g_\ell^2} = \begin{cases} \text{positive}, \quad \text{for } \mathrm{Re}(g_\ell^2) < 1 \\ \\ -i \, \mathrm{sgn}\,(g_\ell \, \omega) \sqrt{g_\ell^2 - 1} \ , \quad \text{for } \mathrm{Re}(g_\ell^2) > 1 \ . \end{cases} \tag{27}$$

(We adopt the convention of positive frequencies, so that $\omega > 0$.)

Next, we proceed to construct the entire solution for $\phi_\ell(x_\ell)$. In the region where $x_\ell < -1/2$, the solution that is well-behaved as $x_\ell \to -\infty$, takes the form $\phi_\ell(x_\ell) \to C^L_\ell [\ln \left| x_\ell + \frac{1}{2} \right| + \Delta_\infty]$ as $x_\ell \to -1/2$. The solution in the intermediate region $-1/2 < x_\ell < 1/2$ is, in general, a superposition of symmetric and antisymmetric components: $\phi_\ell = \lambda_\ell \, \phi^s_\ell + (1-\lambda_\ell) \phi^a_\ell$, with the relative ratio λ_ℓ to be determined. As $x_\ell \to -1/2$, this intermediate solution should behave as

$$\phi_\ell(x_\ell) \to C^L_\ell \left[\ln \left| x_\ell + \frac{1}{2} \right| + \lambda_\ell \, \Delta_s + (1-\lambda_\ell) \Delta_a \right] \ . \tag{28}$$

Then, as $x_\ell \to 1/2$, this intermediate solution behaves as

$$\phi_\ell(x_\ell) \to C^R_\ell \left[\ln \left| x_\ell - \frac{1}{2} \right| + \frac{\lambda_\ell \, \Delta_s - (1-\lambda_\ell) \Delta_a}{2\lambda_\ell - 1} \right] \ , \tag{29}$$

with $C_\ell^R = (2\lambda_\ell - 1)C_\ell^L$. Finally in the region where $x_\ell > 1/2$, the solution that is well-behaved as $x_\ell \to +\infty$, takes the form $\phi_\ell(x_\ell) \to C_\ell^R [\ln|x_\ell - 1/2| + \Delta_\infty]$ as $x_\ell \to 1/2$.

If we now apply the jump conditions at the two gaps, respectively, and eliminate λ_ℓ, we obtain

$$J_\ell^L = C_\ell^L [\lambda_\ell \Delta_s + (1-\lambda_\ell)\Delta_a - \Delta_\infty] = \pi \left(\tilde{\Delta}_\ell C_\ell^R - \overline{\Delta}_\ell C_\ell^L\right) \tag{30}$$

$$J_\ell^R = C_\ell^R \left[\Delta_\infty - \frac{\lambda_\ell \Delta_s - (1-\lambda_\ell)\Delta_a}{2\lambda_\ell - 1}\right] = \pi \left(\overline{\Delta}_\ell C_\ell^R - \tilde{\Delta}_\ell C_\ell^L\right) , \tag{31}$$

where we have defined the following quantities:

$$\overline{\Delta}_\ell \equiv \frac{1}{2\pi}[2\Delta_\infty - (\Delta_s + \Delta_a)] , \quad \tilde{\Delta}_\ell \equiv \frac{1}{2\pi}(\Delta_s - \Delta_a) . \tag{32}$$

Note that in this discussion $\Delta_\infty, \Delta_a, \Delta_s, \overline{\Delta}_\ell$, and $\tilde{\Delta}_\ell$ are all functions of S_ℓ, the local value of the shear. In Table I we list the values of the two quantities $\overline{\Delta}_\ell$ and $\tilde{\Delta}_\ell$ for various values of the shear S_ℓ; observe that $\overline{\Delta}_\ell > 0$, $\tilde{\Delta}_\ell < 0$, and $\overline{\Delta}_\ell/|\tilde{\Delta}_\ell| > 1$. By introducing the expressions of Eqs. (24) and (25) for the jumps into Eqs. (30) and (31), we obtain

$$\alpha_\ell C_\ell^L + \beta_\ell C_{\ell-1}^R = \tilde{\Delta}_\ell C_\ell^R - \overline{\Delta}_\ell C_\ell^L , \tag{33}$$

$$-\alpha_{\ell+1} C_\ell^R - \beta_{\ell+1} C_{\ell+1}^L = \overline{\Delta}_\ell C_\ell^R - \tilde{\Delta}_\ell C_\ell^L . \tag{34}$$

Choosing to eliminate the "left" quantities C_ℓ^L in Eqs. (33) and (34), we obtain a three-term recursion relation for the C_ℓ's at the "right-hand" gaps:

$$\left[\frac{\beta_{\ell+1}^2 - (\alpha_{\ell+1} + \overline{\Delta}_\ell)^2}{\alpha_{\ell+1} + \overline{\Delta}_\ell} + \frac{\tilde{\Delta}_\ell^2}{\alpha_\ell + \overline{\Delta}_\ell}\right] C_\ell = \left(\frac{\beta_\ell \tilde{\Delta}_\ell}{\alpha_\ell + \overline{\Delta}_\ell}\right) C_{\ell-1} + \left(\frac{\beta_{\ell+1}\tilde{\Delta}_\ell}{\alpha_{\ell+1} + \overline{\Delta}_\ell}\right) C_{\ell+1} , \tag{35}$$

where it is henceforth to be understood that C_ℓ means C_ℓ^R.

When the magnitude of g_ℓ^2 becomes larger than unity for real g_ℓ, the square root $(1-g_\ell^2)^{1/2}$, which is contained in the quantities α_ℓ and β_ℓ, becomes imaginary in accordance with the prescription in Eq. (27). This imaginary response is the manifestation of continuum damping of the eigenmode. When g_ℓ lies in the complex plane, the appropriate analytic continuation

for the square root $(1 - g_\ell^2)^{1/2}$ must be taken. A plausible choice for the branch cuts consists of the vertical lines from $g_\ell = \pm 1$ down to $g_\ell = \pm 1 - i\infty$. In a subsequent publication we will show that non-MHD physics, such as the electron response to $E_{||}$ and finite ion Larmor radius effects, determine how the branch cuts emanate from the branch points at $g_\ell = \pm 1$ and go to infinity in the lower-half complex g_ℓ-plane.

III. Solution of the Finite Difference Eigenmode Equation

By means of the matching procedure described in Sec. II, we have effectively replaced the continuous differential eigenmode equation, Eq. (7), which couples the harmonics ϕ_ℓ and $\phi_{\ell\pm1}$, with a finite difference equation, Eq. (35), which couples the amplitudes C_ℓ and $C_{\ell\pm1}$. Equation (35) is now the basic equation to be solved for the eigenvalue g_0. For our initial study we shall assume that we can use S_0 for all S_ℓ and that Eq. (12) is a sufficiently accurate expression for g_ℓ. The former approximation requires that $\frac{\ell}{n}\left(\frac{\partial}{\partial q_\ell} \ln S_\ell\right) \ll 1$ for all sideband numbers ℓ that contribute to the eigenmode, and the latter requires $\epsilon_\ell\, g_\ell \ll 1$. With these approximations $\overline{\Delta}_\ell$ and $\tilde{\Delta}_\ell$ are nearly independent of ℓ, and so we shall suppress the S_ℓ dependence. Also, we shall assume C_ℓ becomes extremely small for large $|\ell|$ and then stretch the domain of ℓ to $-\infty < \ell < \infty$, with the boundary condition $C_\ell \to 0$ as $|\ell| \to \infty$.

The recursion relation, Eq. (35), now has the symmetry property that if a particular eigenvalue g_0 is found, then $g_0 + 2j/m_0\hat{\epsilon}$ for any integer j is also an eigenvalue, with the eigenvector $C_\ell \to C_{\ell+j}$. Note that the imaginary part of the eigenvalue g_0 is invariant.

It is fairly straightforward to solve the difference equation (35) numerically. It is also possible to solve Eq. (35) analytically in two interesting limiting cases. The numerical results are found to agree quite well with the analytical solutions, and we now proceed to describe how to derive the latter.

A. Solution in the limit of $m_0\hat{\varepsilon} \ll 1$

This limit corresponds to the case when radially adjacent frequency gaps are strongly mismatched with each other. Hence, an eigenfrequency that lies within a given gap will intersect the shear Alfvén continuum at all other gaps.

In this limit, we have $|g_\ell| \gg 1$ for all ℓ except $\ell = 0$, for which we assume $g_0 = \mathcal{O}(1)$. Applying the causality condition given in Eq. (27), we find that $\alpha_\ell \to i$ and $\beta_\ell \to 0$ for all $\ell \neq 0$. Only α_0 and β_0 are real. In this case, only the coefficients C_0 and C_{-1} are nonzero, and the three-term recursion relation of Eq. (35) reduces to a two-by-two determinant, which yields the following result for $g_0^{(0)} \equiv \lim_{m_0\hat{\varepsilon}\to 0}(g_0)$:

$$g_0^{(0)} = -\left(\frac{1-y^2}{1+y^2}\right) , \qquad \text{with} \quad y = \overline{\Delta} - \left(\frac{\tilde{\Delta}^2}{\overline{\Delta} - i}\right) . \tag{36}$$

The results of solving for $\mathrm{Re}\left(g_0^{(0)}\right)$ and $\mathrm{Im}\left(g_0^{(0)}\right)$ as functions of the shear $S = S_0$ are presented graphically in Fig. 2 and tabularly in Table I.

In the small and large shear limits, using the analytic forms for $\overline{\Delta}$ and $\tilde{\Delta}$ given in Table I, we find the following explicit results for the $m_0\hat{\varepsilon} \ll 1$ case:

$$\mathrm{Re}\left(g_0^{(0)}\right) \cong -1 + \left(\frac{\pi^2}{8}\right) S^2 \quad \text{and} \quad \mathrm{Im}\left(g_0^{(0)}\right) \cong -\pi S \exp\left(-\frac{2}{S}\right) \quad \text{when} \quad S \ll 1 \, ; \tag{37}$$

$$\mathrm{Re}\left(g_0^{(0)}\right) \cong 1 \quad \text{and} \quad \mathrm{Im}\left(g_0^{(0)}\right) \cong -\frac{\pi S}{2} \quad \text{when} \quad S \gg 1 \, . \tag{38}$$

The damping is exponentially small when the shear is small.

B. Solution in the limit of $m_0\hat{\varepsilon} \gg 1$

In the $m_0\hat{\varepsilon} \gg 1$ limit, radially adjacent frequency gaps are nearly aligned with each other over an extended region. Hence, an eigenfrequency that lies within a given gap will also pass through a number of adjacent gaps on both sides before eventually intersecting the shear Alfvén continuum and experiencing dissipation. Although each individual harmonic has only

a limited radial extent, pair-wise coupling that is induced by toroidicity at successive gaps permits the broad excitation of a TAE mode.

In the limit $m_0\hat{\varepsilon} \gg 1$, the coefficients in Eq. (35) vary only slightly with ℓ since $g_{\ell+1} - g_\ell \equiv g'_\ell = 2/m_0\hat{\varepsilon} \ll 1$. Therefore, our method of solution will be a finite-difference variant of WKB theory. Let $C_\ell/C_{\ell-1} = \exp(ik_\ell)$ and expand $k_\ell = k_\ell^{(0)} + g'_\ell k_\ell^{(1)} + \cdots$. To lowest order in the expansion parameter g'_ℓ, we evaluate all the coefficients in Eq. (35) at the same value of ℓ, and we also approximate $k_{\ell+1} \cong k_\ell^{(0)}$ as slowing varying. This yields

$$\cos k_\ell^{(0)} = f(g_\ell) \ , \qquad \text{with} \quad f_\ell = -\frac{\overline{\Delta}}{\widetilde{\Delta}}\, g_\ell - \frac{(1 - \overline{\Delta}^2 + \widetilde{\Delta}^2)}{2\widetilde{\Delta}} \sqrt{1 - g_\ell^2} \ , \tag{39}$$

or

$$\exp(ik_\ell^{(0)}) = f_\ell \pm \sqrt{f_\ell^2 - 1} \ . \tag{40}$$

For $|f_\ell| < 1$, the C_ℓ coefficients exhibit wave-like oscillatory behavior, as can be seen from writing C_ℓ in the following form:

$$C_\ell = e^{ik_\ell}\, e^{ik_{\ell-1}}\, e^{ik_{\ell-2}} \cdots \cong \exp\left(i \sum_j^\ell k_j^{(0)} \right) \cong \exp\left[i \int^{\ell+1/2} d\ell' \cos^{-1} f(\ell') \right] \ . \tag{41}$$

For $|f_\ell| > 1$, the quantity $k_\ell^{(0)}$ becomes imaginary and solutions are predicted for the C_ℓ that either grow or decay as $|\ell| \to \infty$. We must choose the decaying solution, which corresponds to the minus sign in Eq. (40).

This lowest-order analysis shows that there are two turning points, located where $f_\ell = \pm 1$. Let $g_\ell^\pm$ be the two values of g_ℓ for which this happens. Figure 3 shows a graph of f_ℓ as a function of g_ℓ, for $S = 0.8$. Because $-\overline{\Delta}/\widetilde{\Delta} > 1$, it can easily be proved that $|g_\ell^\pm| < 1$. Therefore the continuum resonance points $g_\ell = \pm 1$ occur in the evanescent region where $f_\ell^2 > 1$ and where the C_ℓ have already exponentially decreased from their levels in the wave-like region (where $f_\ell^2 < 1$), as illustrated schematically in Fig. 4. Hence it is reasonable to expect that the continuum damping rate will be proportional to a combination of the tunneling factors $\exp\left(\mp 2 \int_{g^\pm}^{\pm 1} \frac{dg}{g'} \cosh^{-1}|f_\ell|\right)$, evaluated from the wave-like region to the evanescent region.

To be able to calculate the damping rate accurately, we also need to solve the mode equation to next order in g'_ℓ. Here a difficulty arises, in that Eq. (35) is singular when $\alpha_\ell + \overline{\Delta} = 0$. This singularity occurs in the evanescent region, for a value of g_ℓ between the turning point at $g_\ell = g_\ell^+$ and the continuum resonance point at $g_\ell = 1$. It is possible to seek a solution of the finite difference equation, Eq. (35), that avoids this singular behavior. The derivation is somewhat complicated and is presented in the Appendix. Here we quote the solution for $f_\ell > 1$:

$$C_\ell = \Gamma \frac{\left(g_\ell - \overline{\Delta}\sqrt{1-g_\ell^2}\right)\left(f_\ell - \sqrt{f_\ell^2-1}\right)}{(f_\ell^2-1)^{1/4}\left[1+\tilde{\Delta}\sqrt{1-g_\ell^2}\left(f_\ell-\sqrt{f_\ell^2-1}\right)\right]} \exp\left[-\int_{g_\ell^+}^{g_\ell}\frac{dg}{g'}\ln\left(f+\sqrt{f^2-1}\right)\right] . \tag{42}$$

In Eq. (44), Γ is a normalization constant, and all quantities are evaluated at ℓ. Notice that in the wave-like region (where $f_\ell^2 < 1$), Eq. (42) yields

$$C_\ell = 2\Gamma \frac{\left(\overline{\Delta}\sqrt{1-g_\ell^2} - g_\ell\right)^{1/2}}{(1-f_\ell^2)^{1/4}} \cos\left[\int_{g_\ell}^{g_\ell^+}\frac{dg}{g'}(\cos^{-1} f) - \frac{\pi}{4}\right] . \tag{43}$$

The usual WKB joining condition applies at the turning points $f_\ell = \pm 1$.

Having obtained the wavefunction, we now calculate the damping rate, using a quadratic form for Eq. (35) that is constructed by multiplying the equation by C_ℓ^* and summing over all ℓ:

$$I = \sum_\ell |C_\ell^2|\left(\frac{1+\overline{\Delta}^2}{\overline{\Delta}+\alpha_{\ell+1}} - 2\overline{\Delta}\right) + \sum_\ell |C_{\ell+1}^2|\left(\frac{\overline{\Delta}^2}{\overline{\Delta}+\alpha_{\ell+1}}\right) - \sum_\ell 2\,\mathrm{Re}\left(C_\ell\, C_{\ell+1}^*\right)\left(\frac{\beta_{\ell+1}\tilde{\Delta}}{\overline{\Delta}+\alpha_{\ell+1}}\right) = 0 . \tag{44}$$

For real g_ℓ, the quadratic form I will have an imaginary part that arises from α_ℓ and β_ℓ when $g_\ell^2 \geqq 1$, in the resonance region. The main contribution in this region will come from values of $|g_\ell|$ close to unity, since for large $m_0\hat{\varepsilon} \gg 1$, C_ℓ decreases rapidly as $|g_\ell|$ increases. In this region, we have $f_\ell \cong -g_\ell\overline{\Delta}/\tilde{\Delta}$ and, for $|g_\ell| > 1$,

$$|C_\ell|^2 = \frac{\Gamma^2}{(f_\ell^2-1)^{1/2}} \exp\left(-\frac{2H_\pm}{g'_\ell}\right) \exp\left[-2\ln\left(|f_\ell| + \sqrt{f_\ell^2-1}\right)\frac{(|g_\ell|-1)}{g'_\ell}\right] , \tag{45}$$

with

$$H_{\pm} = \int_{|g^{\pm}|}^{1} d|g| \, \ln\left(|f| + \sqrt{f^2 - 1}\right) \tag{46}$$

where $g_\ell^{\pm}$ are the values of g_ℓ for which $f_\ell = \pm 1$. Now collect the imaginary parts of I, for $|g_\ell|$ close to unity, to find

$$\mathrm{Im}(I) = -\,\mathrm{Im}\sum_{\ell}\left\{\left[\left|C_\ell^2\right|(1+\overline{\Delta}^2) + \left|C_{\ell+1}^2\right|\tilde{\Delta}^2\right]\left(\frac{\sqrt{1-g_\ell^2}}{g_\ell}\right) + 2\,|C_\ell\, C_{\ell+1}|\,\tilde{\Delta}\overline{\Delta}\sqrt{1-g_\ell^2}\right\} . \tag{47}$$

Then, applying Eq. (27) for $|g_\ell|^2 > 1$, we obtain

$$\begin{aligned}\mathrm{Im}(I) &= \sum_{\ell}\sqrt{g_\ell^2-1}\left\{\left[|C_\ell|^2(1+\overline{\Delta}^2) + \left|\tilde{\Delta}C_{\ell+1} + \overline{\Delta}g_\ell\, C_\ell\right|^2\right] - \overline{\Delta}^2|C_\ell|^2\right\} \\ &= \sum_{\ell}\sqrt{g_\ell^2-1}\,|C_\ell|^2(1+\overline{\Delta}^2-\tilde{\Delta}^2) .\end{aligned} \tag{48}$$

Approximately converting the sum in Eq. (48) to an integral [see Sec. III.C for a better treatment] and using Eq. (45), we find

$$\mathrm{Im}(I) = \Gamma^2\sqrt{g'}\,\frac{\frac{\sqrt{\pi}}{4}\left[\exp\left(-\frac{2H_+}{g'}\right) + \exp\left(-\frac{2H_-}{g'}\right)\right]}{\left(\frac{\overline{\Delta}^2}{\tilde{\Delta}^2}-1\right)^{1/2}\left[\ln\left(\left|\frac{\overline{\Delta}}{\tilde{\Delta}}\right| + \sqrt{\frac{\overline{\Delta}^2}{\tilde{\Delta}^2}-1}\right)\right]^{3/2}} \tag{49}$$

where we have added the damping from the two dissipative regions $g_\ell > 1$ and $g_\ell < -1$.

The damping rate can finally be determined from the relationship

$$\mathrm{Im}(g_0)\,\frac{\partial I}{\partial g_0} + \mathrm{Im}(I) = 0 . \tag{50}$$

Assuming that g_ℓ is slowly varying in ℓ, we can rewrite Eq. (44) as

$$I = \sum_{\ell}\left(\frac{\beta\tilde{\Delta}}{\overline{\Delta}+\alpha}\right)\left[|C_\ell^2|2f - \left(C_\ell\, C_{\ell+1}^{*} + C_\ell^{*}\, C_{\ell+1}\right)\right] . \tag{51}$$

Equation (51) is a variational expression for real g_0, which vanishes to lowest order term by term by virtue of Eq. (39), since $C_\ell \propto \cos\theta_\ell$ and $C_{\ell+1} \propto \cos(\theta_\ell + k_\ell^{(0)})$, with θ_ℓ a rapid function of ℓ. Hence, in evaluating the derivative $\partial I/\partial g$ required in Eq. (50), we need only

differentiate f, since the derivative of other quantities will still be multiplied by terms that vanish. Hence, using Eq. (43), we find:

$$\frac{\partial I}{\partial g} = 2\int \left(\frac{\beta\tilde{\Delta}}{\overline{\Delta}+\alpha}\right)|C_\ell|^2 \frac{\partial f}{\partial g}\frac{dg}{g'} = -\Gamma^2 \frac{2\tilde{\Delta}}{g'}\int_{-1}^{+1}\frac{df}{\sqrt{1-f^2}}(2\cos\theta_0)^2 \cong -\frac{4\pi|\tilde{\Delta}|\Gamma^2}{g'} \ . \quad (52)$$

In the large $m_0\tilde{\varepsilon}$ limit, we have neglected contributions to I from $|f|>1$.

Finally, combining Eqs. (49), (50), and (52), we obtain an expression for the damping rate $\mathrm{Im}(g_0^{as}) \equiv \lim_{m_0\hat{\varepsilon}\gg 1}\mathrm{Im}(g_0)$:

$$\mathrm{Im}(g_0^{as}) = \frac{2}{\varepsilon}\left(\frac{\mathrm{Im}\,\omega}{\omega}\right) = -\frac{G(S)}{(m_0|\hat{\varepsilon}|)^{3/2}}\left[\exp(-m_0\hat{\varepsilon}H_+)+\exp(-m_0\hat{\varepsilon}H_-)\right] \ , \quad (53)$$

with

$$G(S) = \frac{\sqrt{2}}{8\sqrt{\pi}}\frac{(1+\overline{\Delta}^2-\tilde{\Delta}^2)}{\sqrt{\overline{\Delta}^2-\tilde{\Delta}^2}}\left[\ln\left(\frac{\overline{\Delta}}{|\tilde{\Delta}|}+\sqrt{\frac{\overline{\Delta}^2}{|\tilde{\Delta}|^2}-1}\right)\right]^{-3/2} \ . \quad (54)$$

The functions G, H_+, and H_- depend only on the value of the shear S. The integrals $H_\pm$ defined in Eq. (46) can be performed in terms of standard elliptic integrals:

$$H_\pm(S) = \cosh^{-1}B - \frac{B\sqrt{B^2-1}}{A^2+B^2} + \frac{|A|}{A^2+B^2}\left[F(k,\varphi)-E(k,\varphi)\right] - \frac{(\pm A)}{\sqrt{A^2+B^2}}\left[K(k)-E(k)\right] \ . \quad (55)$$

Here, we have defined

$$A = \frac{1-\overline{\Delta}^2+\tilde{\Delta}^2}{2\tilde{\Delta}} \ , \ B = -\frac{\overline{\Delta}}{\tilde{\Delta}} \ , \ k^2 = \frac{A^2+B^2-1}{A^2+B^2} \ , \ \varphi = \sin^{-1}\left(\frac{|A|}{\sqrt{A^2+B^2-1}}\right) \ , \quad (56)$$

with $F(k,\varphi)$ and $E(k,\varphi)$ the usual elliptic integrals of the first and second kinds, and $K(k) = F(k,\pi/2)$ and $E(k) = E(k,\pi/2)$ the usual complete elliptic integrals of the first and second kinds.

C. Comparison of numerical and analytical results

In the preceding two subsections, we derived analytic expressions for the continuum damping rate in the two limits of $m_0\hat{\varepsilon} \ll 1$ and $m_0\hat{\varepsilon} \gg 1$. The former is given in Eq. (36) and the

latter in Eq. (53). An interpolation formula for the entire range of $m_0\hat{\varepsilon}$ is

$$\frac{1}{\mathrm{Im}(g_0)} = \frac{1}{\mathrm{Im}\left(g_0^{(0)}\right)} + \frac{1}{\mathrm{Im}(g_0^{as})} \,. \tag{57}$$

Since damping given by Eq. (53) decreases as $m_0\hat{\varepsilon}$ increases, this interpolation formula, Eq. (57), provides an estimate for the upper limit of the damping at a given shear S.

Figure 5 shows the results obtained from a direct numerical solution of the finite difference eigenmode equation, Eq. (35), for $S = 0.8$. The results for other S values show the same qualitative features. One interesting result in the appearance of intervals in $m_0\hat{\varepsilon}$ where solutions are not found as roots disappear or emerge from the branch cuts in the complex g_ℓ-plane. In Fig. 5(a) the shaded regions indicate the intervals in $m_0\hat{\varepsilon}$ within which roots are not found.

The analytical results indicated by the dashed curves in Figs. 5(a) and 5(b) exhibit good agreement with the numerical results (solid curves) at large and even moderate values of $m_0\hat{\varepsilon}$ and also at $m_0\hat{\varepsilon} \to 0$. The good correspondence occurs in spite of the fact that justification of the WKB type of analysis in the large $m_0\hat{\varepsilon}$ limit formally requires that the exponentially decaying region between the wave-like and dissipative regions be large. In contrast to the analytical results, the numerical results for the damping rate do exhibit significant oscillation as $m_0\hat{\varepsilon}$ is varied. However, this may be expected from the discretized nature of the summation for $\mathrm{Im}(I)$ in Eq. (44). Also, at small shear and small values for $m_0\hat{\varepsilon}$, these oscillations are enhanced because in the numerical routine, the sign of the quantity $(1-g_\ell^2)^{1/2}$ is discontinuously changed when branch cuts are crossed. In the analysis described in this paper, the branch cuts were taken to run from the singular points $g_\ell = \pm 1$ down to $g_\ell = \pm 1 - i\infty$. The introduction of finite resistivity and gyroradius effects into the theory leads to a self-consistent determination of the branch cuts and their contribution.

It is possible analytically to describe the oscillations in the damping rate and thus further improve the comparison between the analytical and numerical results by taking into account

the discrete nature of the summation in Eq. (44) for $\mathrm{Im}(I)$, which in turn determines the damping rate $\mathrm{Im}(g_0)$ through Eq. (50). We found that

$$\mathrm{Im}(I) \propto \sum_{\ell>\ell_+}^{\infty} |C_\ell|^2 (g_\ell - 1)^{1/2} + \sum_{\ell<\ell_-}^{\infty} |C_\ell|^2 |g_\ell + 1|^{1/2} \ , \tag{58}$$

where the values $\ell_\pm$ are defined by the resonance condition $g(\ell_\pm) = \pm 1$, so that

$$\ell_\pm = \frac{1}{2} m_0 \hat{\varepsilon} [\pm 1 - \mathrm{Re}(g_0)] \ . \tag{59}$$

The summation in Eq. (58) is over integer ℓ values. For the amplitude C_ℓ in Eq. (58), we used the approximation

$$|C_\ell|^2 \cong \left| C_{\ell_+} \exp\left[i \int_{\ell_+}^{\ell} d\ell' k(\ell') \right]^2 \right| \cong \left| C_{\ell_+} \exp\left[-\kappa(S)(\ell - \ell') \right] \right|^2 \ , \quad \text{for } \ell > \ell_+ \ , \tag{60}$$

with $\kappa(S) = \cosh^{-1}\left(\dfrac{\overline{\Delta}}{|\tilde{\Delta}|} \right)$, and similarly for $\ell < \ell_-$. Hence, the evaluation of $\mathrm{Im}(I)$ requires the summation

$$\begin{aligned} \mathrm{Im}(I) \ &\propto \ |C_{\ell_+}|^2 \sum_{\ell=\mathrm{Int}(\ell_+)+1}^{\infty} (\ell - \ell_+)^{1/2} \exp\left[-2\kappa(S)(\ell - \ell_+) \right] \\ &+ \ |C_{\ell_-}|^2 \sum_{\ell=\mathrm{Int}(|\ell_-|)+1}^{\infty} (\ell - |\ell_-|)^{1/2} \exp\left[-2\kappa(S)(\ell - |\ell_-|) \right] \end{aligned} \tag{61}$$

where $\mathrm{Int}(p)$ is the integer part of p. The difference $\delta\ell^\pm$ between where the resonance occurs at $\ell = \ell_\pm$ (with ℓ here treated as if it were a continuous variable) and where the summation begins, is

$$\delta\ell^\pm = \mathrm{Int}(|\ell_\pm|) + 1 - |\ell_\pm| \ , \tag{62}$$

where $\delta\ell^\pm$ ranges in value from zero to unity. Observe that $\mathrm{Im}(I)$, if uniformly averaged over all possible values for $\delta\ell^\pm$, yields the result that would be obtained if the summation were replaced by a continuous integral:

$$\langle \mathrm{Im}(I) \rangle \ \equiv \ \int_0^1 d(\delta\ell^\pm) |C_{\ell_\pm}|^2 \sum_{\ell=|\ell_\pm|+\delta\ell^\pm}^{\infty} (\ell - |\ell_\pm|)^{1/2} \exp\left[-2\kappa(S)(\ell - |\ell_\pm|) \right]$$

$$= |C_{\ell_\pm}|^2 \sum_{n=0}^{\infty} \int_n^{n+1} dy \sqrt{y} \exp[-2\kappa(S)y]$$
$$= \frac{\sqrt{\pi}}{4\sqrt{2}\,\kappa^{3/2}} |C_{\ell_\pm}|^2 \,. \tag{63}$$

In deriving the analytic expression of Eq. (53) for the damping rate, we assumed that the summation in Eq. (48) could be replaced by an integral. Now, however, we understand that this procedure is justified only in an average sense for uniformly distributed values of $\delta\ell^{\pm}$. The large oscillations in the ratio of the analytical and numerical results as a function of $m_0\hat{\varepsilon}$ are a reflection of the loss of phase information when a discrete sum is modelled by an integral.

In order to capture the oscillatory dependence of the damping rate with $\delta\ell^{\pm}$, we introduce the following phase factor:

$$F(\kappa(S), \delta\ell^{\pm}) = \frac{4\sqrt{2}\,\kappa^{3/2}}{\sqrt{\pi}} \sum_{n=0}^{\infty} \sqrt{n + \delta\ell^{\pm}} \exp[-2\kappa(S)(n + \delta\ell^{\pm})] \,, \tag{64}$$

with $0 \leq \delta\ell^{\pm} \leq 1$. The functional dependence of $F(\kappa, \delta\ell^{\pm})$ on $\delta\ell^{\pm}$ for various values of the shear is shown in Fig. 6. We modify the expression in Eq. (55) for the damping rate to include this oscillatory phase information, as follows:

$$\mathrm{Im}(g_0) = -\frac{G(S)}{(m_0|\hat{\varepsilon}|)^{3/2}} \left[F(\kappa, \delta\ell^{+}) \exp(-m_0\hat{\varepsilon}H_{+}) + F(\kappa, \delta\ell^{-}) \exp(-m_0\hat{\varepsilon}H_{-}) \right] \,. \tag{65}$$

The appropriate values for the quantities $\delta\ell^{\pm}$, defined in Eq. (62), that should be used in Eq. (65) have, in fact, been determined from our knowledge of the real part of g_0 obtained from the numerical solution of Eq. (35), although in principle it would be possible to use the WKB condition $\sum_{\ell} \cos^{-1} f_\ell = (N + \frac{1}{2})\pi$, for integral N, to determine g_0 analytically. Figure 7 shows a comparison of the numerical results for $\mathrm{Im}(g_0)$ with the analytical results calculated from Eq. (65). Clearly, the oscillatory behavior of the damping rate that was seen in Fig. 5 has been largely reproduced. Moreover, by fitting a curve through the maximum values of the ratio of the numerical and analytical results, we find asymptotic convergence

of the form

$$\text{Max}\left[\frac{\text{Im}(g_0)_{\text{Numerical}}}{\text{Im}(g_0)_{\text{Analytical}}}\right] \cong 1 - (2.0 \pm 0.1)(m_0\hat{\varepsilon})^{-2/3} \ . \tag{66}$$

D. Extension to broad eigenfunctions

If the poloidal harmonics are sufficiently extended, it is no longer valid to use the approximations $S_\ell = S_0$ and $g_\ell = g_0 + 2\ell/m_0\hat{\varepsilon}$. We need to return to the more accurate finite difference scheme given by Eq. (35), where the shear may vary from gap to gap, although remaining locally "frozen" near individual gaps. The WKB procedure of Sec. III.B may be generalized to this case, but the results for G and $H_\pm$ are complicated numerical integrals. Here we report on direct numerical integration of Eq. (35). The values of $\overline{\Delta}_\ell$ and $\tilde{\Delta}_\ell$ as functions of the local value of the shear $S_\ell = S(r_\ell)$ at each gap can be computed and stored before Eq. (35) is solved. The value of $m \equiv m_0 + \ell$ is taken to range from m_0 to $m_0 + L_{\max}$, where $m_0 < nq(0) < m_0 + 1$ and $L_{\max} + m_0 - 1 < nq(a) < L_{\max} + m_0$. For boundary conditions we use

$$C_{L_{\max}} = 0 \qquad \text{and} \qquad -\frac{C_1}{C_0}\tilde{\Delta}(S_1)\beta_1 + 1 - 2\alpha_1\overline{\Delta}(S_1) - \overline{\Delta}^2(S_1) = 0 \ . \tag{67}$$

The latter boundary condition follows from requiring that $\tilde{\Delta}(S_{-1}) = 0$ and that the value of $\overline{\Delta}(S_\ell)$ is insensitive to boundary conditions when $S_\ell \ll 1$, which is the case near the axis.

The solution of Eq. (35) was carried out with the following choice of equilibrium profiles:

$$q(r) = q_0 + [q(a) - q(0)]\left(\frac{r}{a}\right)^2 \ , \qquad \rho(r) = \rho(0)\left[1 - \left(\frac{r}{a}\right)^4\right] \ . \tag{68}$$

The results are shown in Fig. 8 for $n = 3$, $a/R = 0.20$, $q(0) = 1.0$, and $q(a) = 3.0$. There are many eigenvalues, roughly one for each gap. The harmonic content $|C_\ell|^2$ of the global TAE mode associated with each of these discrete eigenfrequencies is shown in Fig. 9 as a bar plot of $|C_\ell|^2$ versus sideband number ℓ. Observe that there is a tendency for most of the eigenmodes to excite a cluster of harmonics at those values of ℓ where $\frac{\partial}{\partial q^2}\ln(q^2/v_A^2)$ is small. In Table II we tabulate the eigenvalues obtained for the case of $n = 10$, for the

same equilibrium. The damping rate tends to be smaller than that for the $n = 3$ case. Our analytical expression in Eq. (53) suggests that the damping rate should decrease with mode number as $n^{-3/2}$; however, because of the considerable phase oscillations, this is only a rough estimate.

IV. Discussion

In the present paper, it was shown how for large mode numbers and small inverse aspect ratio ($n \gg 1$ and $\varepsilon \ll 1$, but $n\varepsilon$ still arbitrary), an asymptotically valid finite-difference equation can be derived to describe the TAE eigenmode structure in a large-aspect-ratio circular tokamak geometry. From this difference equation, the shear Alfvén continuum damping for the TAE mode was calculated, both analytically (for $n\epsilon \ll 1$ and for $n\epsilon \gg 1$) and numerically.

The continuum damping rate is found to be significant, unless the shear is small (in which case the damping is exponentially small) or the parameter $\hat{\varepsilon}$ is large (which occurs when the gaps are nearly aligned). For other values, the damping rate is typically a few percent of the oscillation frequency. This is competitive with the alpha particle-excited growth rate for the TAE instability in an ignition tokamak and could help to stabilize or ameleorate this potentially dangerous mode. The stabilizing effect of continuum damping could also be a candidate to explain threshold values observed in recent experiments that excited the TAE instability with neutral beam-injected hot ions.

We can offer a rough formula for the analytical prediction for the continuum growth rate. For typical values, the crude approximations $G(S) \approx 0.8S^2$ and $H_{\pm} \approx 0$ may be used in Eq. (53) to obtain

$$\frac{\gamma}{\omega} \approx -\frac{0.8\varepsilon S^2}{(m_0\hat{\varepsilon})^{3/2}} , \tag{69}$$

accurate to about a factor of two for $S > 0.3$ and $1 < m_0\hat{\varepsilon} < 20$.

Concerning the mode number dependence, we remark that although continuum damping decreases strongly with m_0 and the alpha-particle drive increases with m_0, the latter mechanism can be reduced by finite gyroradius effects and banana effects,[25] and other non-ideal MHD types of damping, e.g., due to a non-zero parallel electric field, will increase with mode number. Thus, it is plausible that intermediate mode numbers — such as those observed in recent TAE experiments — are most dangerous.

We also note that weak continuum damping at low shear values suggests that TAE instability is likely toward the center of the discharge, leading to flattening of the central distribution of alpha particles. The other susceptible region is where $\frac{\partial}{\partial q^2} \ln(q^2/v_A^2)$ changes sign, which, depending on equilibrium profiles, characteristically occurs towards the outer part of the plasma. The likelihood of instability then depends on whether the destabilizing energetic particles extend out to this region.

Acknowledgments

We are grateful to L. Chen, M.S. Chu, and F. Zonca, for useful discussions and to Mr. J. Candy for supplying the more precise values in Table I. This work was supported by the U.S. Department of Energy under contract DE-FG05-80ET-53088 with The University of Texas at Austin and contract DE-FG03-80ER-53275 with the University of California, San Diego.

Appendix A — Non-Singular Solution for C_ℓ

Here we show how to solve the finite difference eigenmode equation, Eq. (35), in the $m_0\widehat{\varepsilon} \gg 1$ limit in such a way as to avoid the singular behavior that occurs when $\alpha_\ell + \overline{\Delta} = 0$ or, equivalently, when $g_\ell = \widehat{g}_\ell$, with $\widehat{g}_\ell = \overline{\Delta}(1+\overline{\Delta}^2)^{-1/2} > 0$. Because $\widehat{g}_\ell < 1$, and because it can be shown that $f(\widehat{g}_\ell) > 1$, we see that this apparent singularity lies in the non-dissipative part of the evanescent region, i.e., $g_\ell^+ < \widehat{g}_\ell < 1$.

We now seek to transform away the singularity, assuming that the solution for C_ℓ is evanescent at large ℓ. First, we rewrite Eq. (35) as

$$\tilde{\Delta} J_{\ell+1} - \frac{\tilde{\Delta}^2}{\beta_\ell} J_\ell = -Z_{\ell+1}\,\beta_{\ell+1}\,C_\ell \;, \tag{A1}$$

where we have defined

$$J_{\ell+1} = \frac{C_{\ell+1} - (\beta_{\ell+1}/\tilde{\Delta})\,C_\ell}{Z_{\ell+1}} \tag{A2}$$

with

$$Z_\ell \equiv \frac{\alpha_\ell + \overline{\Delta}}{\beta_\ell} = g_\ell - \overline{\Delta}\sqrt{1-g_\ell^2}\;. \tag{A3}$$

It is convenient to introduce the rescaled dependent variables $\widehat{J}_\ell$ and $\widehat{C}_\ell$ defined by

$$\frac{C_\ell}{\widehat{C}_\ell} = \prod_{j\le\ell}\left(\frac{\beta_j}{\tilde{\Delta}}\right) = \frac{J_\ell}{\widehat{J}_\ell}\;, \tag{A4}$$

so that Eqs. (A1) and (A2) become

$$\widehat{J}_{\ell+1} - \frac{\tilde{\Delta}^2}{\beta_\ell\,\beta_{\ell+1}}\widehat{J}_\ell = -Z_{\ell+1}\,\widehat{C}_\ell \tag{A5}$$

$$\widehat{C}_\ell = \widehat{C}_{\ell+1} - Z_{\ell+1}\,\widehat{J}_{\ell+1}\;. \tag{A6}$$

Notice that all the coefficients in Eqs. (A5) and (A6) are well behaved. Since $C_\ell \to 0$ as $\ell \to \infty$, we can sum Eq. (A6) and obtain (for $\ell > 0$)

$$\widehat{C}_\ell = -\sum_{n=\ell+1}^{\infty} Z_n \widehat{J}_n\;. \tag{A7}$$

If we take $Q_\ell = \frac{\widehat{J}_{\ell+1}}{\widehat{J}_\ell}$, Eqs. (A6) and (A7) become

$$Q_\ell - \frac{\widetilde{\Delta}^2}{\beta_\ell \beta_{\ell+1}} = Z_{\ell+1} \sum_{p=0}^{\infty} \left[Z_{p+\ell+1} \left(\prod_{n=0}^{p} Q_{n+\ell} \right) \right] \tag{A8}$$

and

$$\widehat{C}_\ell = \widehat{J}_\ell \sum_{p=0}^{\infty} \left[Z_{p+\ell+1} \left(\prod_{n=0}^{p} Q_{n+\ell} \right) \right] . \tag{A9}$$

We may now assume slow variation with ℓ: $W_{\ell+1} \cong W_\ell + W'_\ell$ and $Q_{\ell+1} \cong Q_\ell + Q'_\ell$, with $|W'_\ell / W_\ell| = \mathcal{O}(m_0 \widehat{\varepsilon})^{-1} \ll 1$. Hence, we may approximately write

$$\begin{aligned} \prod_{n=0}^{p} Q_{n+\ell} &\cong Q_\ell^{p+1} \left(1 + \frac{Q'_\ell}{Q_\ell}\right) \left(1 + \frac{Q'_\ell + Q'_{\ell+1}}{Q_\ell}\right) \cdots \left(1 + \frac{Q'_\ell + Q'_{\ell+1} + \cdots + Q'_{p+\ell-1}}{Q_\ell}\right) \\ &\cong Q_\ell^{p+1} \left[1 + \frac{1}{2} p(p+1) \frac{Q'_\ell}{Q_\ell}\right] \end{aligned} \tag{A10}$$

and

$$Z_{p+\ell+1} \cong Z_\ell + Z'_\ell + Z'_{\ell+1} + \cdots + Z'_{p+\ell} \cong Z_\ell + (p+1) Z'_\ell . \tag{A11}$$

In this way we obtain

$$\sum_{p=0}^{\infty} \left[Z_{p+\ell+1} \left(\prod_{n=0}^{p} Q_{n+\ell} \right) \right] \cong \frac{Z_\ell Q_\ell}{1 - Q_\ell} + \frac{Z_\ell Q_\ell Q'_\ell}{(1 - Q_\ell)^3} + \frac{Z'_\ell Q_\ell}{(1 - Q_\ell)^2} . \tag{A12}$$

Using Eq. (A12), we can rewrite Eq. (A8) as

$$Q_\ell - \frac{\widetilde{\Delta}^2}{\beta_\ell^2} - \frac{Z_\ell^2 Q_\ell}{1 - Q_\ell} \cong - \left(\frac{\widetilde{\Delta}^2}{\beta_\ell^3} \right) \beta'_\ell + \frac{Z_\ell Z'_\ell Q_\ell (2 - Q_\ell)}{(1 - Q_\ell)^2} + \frac{Z_\ell^2 Q_\ell Q'_\ell}{(1 - Q_\ell)^3} . \tag{A13}$$

We can solve Eq. (A13) perturbatively as an expansion $Q_\ell = Q_\ell^{(0)} + Q_\ell^{(1)} + \cdots$, with $\left| Q_\ell^{(1)} / Q_\ell^{(0)} \right| = \mathcal{O}(m_0 \widehat{\varepsilon})^{-1} \ll 1$. The lowest-order solution $Q_\ell^{(0)}$ satisfies Eq. (A13) with the small terms on the right-hand side neglected. Let $Q_\ell = \left(\frac{\widetilde{\Delta}}{\beta_\ell} \right) \widehat{Q}_\ell$; then $\widehat{Q}_\ell^{(0)}$ is given by

$$\widehat{Q}_\ell^{(0)} = f - \sqrt{f^2 - 1} , \tag{A14}$$

with

$$f = \frac{\beta_\ell}{2\widetilde{\Delta}} \left(1 - \frac{\widetilde{\Delta}^2}{\beta_\ell^2} - Z_\ell^2 \right) = - \left(\frac{\overline{\Delta}}{\widetilde{\Delta}} \right) g_\ell - \frac{(1 - \overline{\Delta}^2 + \widetilde{\Delta}^2)}{2\widetilde{\Delta}} \sqrt{1 - g_\ell^2} . \tag{A15}$$

In Eq. (A14), the sign of the square root was chosen so as to have $|\widehat{Q}_\ell^{(0)}| < 1$, assuring an evanescent solution at large ℓ.

With the use of the lowest-order relationship

$$Z_\ell^2 = \left(1 - Q_\ell^{(0)}\right)\left(1 - \frac{\tilde{\Delta}^2}{Q_\ell^{(0)}\beta_\ell^2}\right) , \tag{A16}$$

the next-order solution $Q_\ell^{(1)}$ is obtained from Eq. (A13) as

$$\begin{aligned}\frac{Q_\ell^{(1)}}{Q_\ell^{(0)}} &= \frac{1}{\widehat{Q}_\ell^{(0)}\left(\widehat{Q}_\ell^{(0)} - \frac{1}{\widehat{Q}_\ell^{(0)}}\right)}\left[-\frac{\beta_\ell'}{\beta_\ell} - \frac{\beta_\ell^2}{2\tilde{\Delta}^2}\left(\frac{Q_\ell^{(0)2}Q_\ell^{(0)'}}{1-Q_\ell^{(0)}}\right) + \frac{Q_\ell^{(0)}Q_\ell^{(0)'}\left(\frac{3}{2}Q_\ell^{(0)} - 1\right)}{Q_\ell^{(0)2}\left(1-Q_\ell^{(0)}\right)}\right] \\ &= -\frac{1}{2}\left(\frac{Q_\ell^{(0)'}}{1-Q_\ell^{(0)}}\right) - \frac{\widehat{Q}_\ell^{(0)'}}{\widehat{Q}_\ell^{(0)}\left(\widehat{Q}_\ell^{(0)2} - 1\right)}\end{aligned} \tag{A17}$$

where we used the identity

$$-\frac{\beta_\ell^2}{2\tilde{\Delta}^2}\frac{Q_\ell^{(0)2}Q_\ell^{(0)'}}{\left(1-Q_\ell^{(0)}\right)}\frac{1}{\left(\widehat{Q}_\ell^{(0)2}-1\right)} = -\frac{1}{2}\left(\frac{Q_\ell^{(0)'}}{1-Q_\ell^{(0)}}\right)\left[1 + \frac{1}{\left(1-Q_\ell^{(0)}\right)\left(\widehat{Q}_\ell^{(0)2}-1\right)}\right] . \tag{A18}$$

Then, using the identities $\widehat{Q}_\ell^{(0)2} - 1 = -2\widehat{Q}_\ell^{(0)} - \sqrt{f_\ell^2 - 1}$ and $\widehat{Q}_\ell^{(0)'} = -\widehat{Q}_\ell^{(0)} f_\ell / \sqrt{f_\ell^2 - 1}$ to find

$$\frac{\widehat{Q}_\ell^{(0)'}}{\widehat{Q}_\ell^{(0)}\left(\widehat{Q}_\ell^{(0)2} - 1\right)} = \frac{ff'}{2(f^2-1)} - \frac{\widehat{Q}_\ell^{(0)'}}{2\widehat{Q}_\ell^{(0)}} , \tag{A19}$$

we finally obtain

$$\frac{Q_\ell^{(1)}}{Q_\ell^{(0)}} = \left[\frac{1}{2}\ln\left(1-Q_\ell^{(0)}\right) - \frac{1}{4}\ln(f_\ell^2 - 1) + \frac{1}{2}\ln\widehat{Q}_\ell^{(0)}\right]' . \tag{A20}$$

Now we return to Eq. (A9) and use Eq. (A12) to obtain

$$-\left(\frac{\widehat{C}_\ell}{\widehat{J}_\ell}\right) = \frac{Z_\ell Q_\ell}{1-Q_\ell}\left[1 + \mathcal{O}(m_0\hat{\varepsilon})^{-1}\right] . \tag{A21}$$

Furthermore, we can write

$$\begin{aligned}Q_\ell \widehat{J}_\ell &= \prod_{p\leqq\ell} Q_p = \exp\left(\sum_{p\leqq\ell}\ln Q_p\right) \cong \exp\left[\int^{\ell+\frac{1}{2}} d\bar{\ell}\,\ln Q(\bar{\ell})\right] \\ &\cong \exp\left[\int^{\ell} d\bar{\ell}\left[\ln Q(\bar{\ell}) + \frac{Q'}{2Q}\right]\right]\end{aligned} \tag{A22}$$

where replacing the discrete sum by a continuous integral is asymptotically valid in the limit $m_0\widehat{\varepsilon} \to \infty$. The upper limit of $\ell + \frac{1}{2}$ for the indefinite integral, which reflects the use of the trapezoidal rule, has been shifted back to ℓ through the addition of the small $Q'/2Q$ term to the integrand. Now introduce the known solution for $Q_\ell = Q_\ell^{(0)} + Q_\ell^{(1)}$ into Eq. (A22) to obtain the final result of Eq. (42):

$$C_\ell = -\left[\prod_{j\leq\ell}\left(\frac{\beta_j}{\widetilde{\Delta}}\right)\right]\frac{Z_\ell}{1-Q_\ell^{(0)}}\exp\left\{\int^\ell d\bar{\ell}\left[\ln Q^{(0)} + \left(\frac{Q^{(0)\prime}}{2Q^{(0)}} + \frac{Q^{(1)}}{Q^{(0)}}\right)\right]\right\}$$

$$= -\frac{\left(g_\ell - \overline{\Delta}\sqrt{1-g_\ell^2}\right)\left(f-\sqrt{f^2-1}\right)}{(f^2-1)^{1/4}\left[1+\widetilde{\Delta}\sqrt{1-g_\ell^2}\left(f-\sqrt{f^2-1}\right)\right]^{1/2}}\exp\left[\int^{g_\ell}\frac{dg}{g'}\ln(f-\sqrt{f^2-1})\right]. \tag{A23}$$

Note that the higher-order terms such as $Q_\ell^{(1)}$ and $Q_\ell^{(0)\prime}/2Q_\ell^{(0)}$ were important only within summations, since $\ell \ll m_0$ but $\ell/m_0\widehat{\varepsilon} = \mathcal{O}(1)$. We remark that also for $\ell < 0$, the same expression as in Eq. (A23) is obtained for C_ℓ.

References

1. M.N. Rosenbluth and P. H. Rutherford, Phys. Rev. Lett. **34**, 1428 (1975).

2. A.B. Mikhailovskii, Sov. Phys. JETP **41**, 980 (1975).

3. C.Z. Cheng, L. Chen, and M. S. Chance, Ann. Phys. (N.Y.) **161**, 21 (1984).

4. C.Z. Cheng and M. S. Chance, Phys. Fluids **29**, 3695 (1986).

5. G.Y. Fu, Ph.D. Thesis, The University of Texas at Austin (1988); Institute for Fusion Studies Report, No. IFSR-325 (1988).

6. G.Y. Fu and J. W. Van Dam, Phys. Fluids B **1**, 1949 (1989).

7. L. Chen, in *Theory of Fusion Plasmas 1988*, ed. J. Vaclavik, F. Troyon, and E. Sindoni (Societa Italiana di Fisica/Editrice Compositori, Bologna, 1989), p. 327.

8. D.J. Sigmar, C. T. Hsu, R.B. White, and C.Z. Cheng, submitted to Phys. Fluids B.

9. K.L. Wong, R.J. Fonck, S.F. Paul, D.R. Roberts, E.D. Fredrickson, R. Nazikian, H.K. Park, M. Bell, N.L. Bretz, R. Budny, S. Cohen, G.W. Hammett, F.C. Jobes, D.M. Meade, S.S. Medley, D. Mueller, Y. Nagayama, D.K. Owens, and E.J. Synakowski Phys. Rev. Lett. **66**, 1874 (1991).

10. W.W. Heidbrink, E.J. Strait, E. Doyle, and R. Snider, Nucl. Fusion **31**, 1635 (1991).

11. H.L. Berk and B.N. Breizman, Phys. Fluids B **2**, 2246 (1990).

12. C.Z. Cheng, G.Y. Fu, and J.W. Van Dam, in *Theory of Fusion Plasmas 1988*, ed. J. Vaclavik, F. Troyon, and E. Sindoni (Societa Italiana di Fisica/Editrice Compositori, Bologna, 1989), p. 259.

13. G.Y. Fu, J.W. Van Dam, M.N. Rosenbluth, D.W. Ross, Y.Z. Zhang, H.L. Berk, S. Mahajan, C.Z. Cheng, R.L. Miller, X.H. Wang, A. Bhattacharjee, M.E. Mauel, and B. Breizman, in *Plasma Physics and Controlled Nuclear Fusion Research 1988* (International Atomic Energy Agency, Vienna, 1989), Vol. 2, p. 291.

14. J.W. Van Dam, G.Y. Fu, and C.Z. Cheng, Fusion Technology **18**, 461 (1990).

15. C. Z. Cheng, Fusion Technology **18**, 443 (1990).

16. C.Z. Cheng, Phys. Fluids B **2**, 1427 (1990).

17. C.Z. Cheng, Phys. Fluids B **3**, 2463 (1991).

18. C.Z. Cheng, R.B. White, G.Y. Fu, L. Chen, D.J. Sigmar, C.T. Hsu, A. Beklemishev, H.L. Berk, B. Breizman, S.C. Guo, Z. Guo, D. Lindberg, and J.W. Van Dam, in *Plasma Physics and Controlled Nuclear Fusion Research 1990* (International Atomic Energy Agency, Vienna, 1991), Vol. 2, p. 209.

19. H.L. Berk, J.W. Van Dam, Z. Guo, and D.M. Lindberg, accepted for publication in Phys. Fluids B.

20. S.E. Sharapov and N.N. Gorelenkov, submitted to Physica Scripta.

21. M.N. Rosenbluth, H.L. Berk, D.M. Lindberg, and J.W. Van Dam, accepted for publication in Phys. Rev. Lett.

22. F. Zonca and L. Chen, submitted to Phys. Rev. Lett.

23. D.A. Spong, B.A. Carreras, C.L. Hedrick, P.J. Christenson, L. Charlton, N.A. Dominguez, and J.N. Leboeuf, Bull. Am. Phys. Soc. **36**, 2394 (1991).

24. W. Kerner, S. Poedts, J.P. Goedbloed, G.T.A. Huysmans, B. Keegan, and E. Schwarz, in *18th European Conference on Controlled Fusion and Plasma Physics, Berlin, 3-7*

June 1991 (European Physics Abstracts — European Physical Society, 1991), Vol. 15C, part IV, p. 89.

25. H.L. Berk, B.N. Breizman, and H. Ye, accepted for publication in Phys. Lett.

Figure Captions

1. Toroidally coupled shear-Alfvén continuum resonance curves for the normalized frequency $\omega R/v_{A_0}$ as functions of the normalized minor radius r/a, for $n = 5$, $q(0) = 1.0, q(a) = 2.5$, and $a/R = 0.25$. The m values indicate the dominant mode number in the regions where toroidal coupling is negligible. The horizontal line indicates a TAE eigenfrequency.

2. Solutions for the real and imaginary parts of g_0, as functions of the shear S, in the limit $m_0\hat{\varepsilon} \ll 1$.

3. Graph of f_ℓ versus g_ℓ, for $S = 0.8$. Turning points at $g_\ell = g_\ell^\pm$ occur where $|f_\ell| = 1$, whereas continuum resonance occurs where $|g_\ell| = 1$. Note that $|f_\ell(g_\ell = \pm 1)| = \overline{\Delta}/|\tilde{\Delta}| > 1$.

4. Schematic plots of the toroidal shear Alfvén continuum resonance curves $g_0^{\rm res}(x, \ell)$ and of several TAE harmonics $\phi_\ell(x)$ and their global eigenmode envelope as functions of radial position $x = nq(r) - m_0$.

5. Numerical results (solid curves) and analytical results (dashed curves) for $\mathrm{Im}(g_0)$ as functions of $m_0\hat{\varepsilon}$. The analytical results follow from the interpolation of Eq. (57), and the numerical results from directly solving the three-term recursion relation, Eq. (35). (a) $0 \le m_0\hat{\varepsilon} \le 5$; (b) $5 \le m_0\hat{\varepsilon} \le 25$. Within the intervals shown shaded in (a) and also observable in (b), no roots exist.

6. Dependence of the phase factor $F(\kappa, \delta\ell^\pm)$ of Eq. (64) on $\delta\ell^\pm$ for various values of the shear.

7. Numerical results (solid curve) and analytical results (dashed curve) for $\mathrm{Im}(g_0)$, the latter incorporating the oscillatory phase information in Eq. (65), as functions of $m_0\hat{\varepsilon}$,

for $S = 0.8$.

8. Continuum resonance curves (only the tips of the curves near the gaps are shown) and normalized TAE eigenfrequencies $\omega R/v_{A_0}$, numerically obtained for the profiles of Eq. (68), with $n = 3$, $q(0) = 1$, $q(a) = 3$, and $a/R = 0.2$. The respective eigenfrequencies and their associated damping rates (imaginary part) are A: $(0.52, -4.0 \times 10^{-2})$, B: $(0.40, -8.5 \times 10^{-6})$, C: $(0.35, -1.1 \times 10^{-2})$, D: $(0.34, -3.4 \times 10^{-3})$, E: $(0.31, -4.7 \times 10^{-3})$, and F: $(0.27, -4.0 \times 10^{-3})$.

9. Harmonic content $|C_\ell|^2$ of the global TAE mode associated with each of the discrete eigenfrequencies shown in Fig. 8, for each sideband number ℓ.

Caption for Table I

Values of the $\overline{\Delta}$ and $\tilde{\Delta}$ parameters, the normalized complex frequency $g_0^{(0)}$ of Eq. (36), and the G and $H_\pm$ quantities of Eqs. (56) and (57), as functions of the shear S.

Caption for Table II

Real and imaginary parts of the eigenfrequencies for various TAE modes, along with an indication of the radial spectrum of the mode and the location of the peak of the mode envelope. The numbers listed under "radial spectrum" are the values of $j = (m - n)$ for which the value of $|C_j|^2$ exceeds 10% of the largest such value (located at the bold number in parentheses).

Table I

S	$\overline{\Delta}$	$\tilde{\Delta}$	Re $g_0^{(0)}$	Im $g_0^{(0)}$	G	H_+	H_-
small S	$\pi S/4$	$-\exp(-1/S)$	$-1+\pi^2 S^2/8$	$-(16/\pi S)\exp(-2/S)$	$(S/2)^{1/2}\,\pi^{-3/2}$	$2/S$	$\pi^2\,S/8$
0.3	.2605	-.0621	-.8740	-.00329	.1366	4.515	.09512
0.4	.3831	-.1669	-.7553	-.02797	.1810	2.467	.07606
0.5	.5392	-.3206	-.6065	-.10238	.2337	1.270	.05844
0.6	.7326	-.5190	-.4620	-.2320	.2967	.6250	.04472
0.7	.9650	-.7594	-.3438	-.3968	.3712	.3072	.03455
0.8	1.2369	-1.0405	-.2532	-.5761	.4585	.1560	.02705
0.9	1.5483	-1.3613	-.1835	-.7586	.5594	.08320	.02150
1.0	1.8993	-1.7213	-.12819	-.9404	.6747	.04667	.01733
1.2	2.7193	-2.5578	-.04449	-1.298	.9520	.01686	.01169
1.4	3.6959	-3.5486	.01751	-1.648	1.2970	7.09×10^{-3}	8.24×10^{-3}
1.6	4.8281	-4.6929	.0662	-1.993	1.7161	3.35×10^{-3}	6.02×10^{-3}
1.8	6.1153	-5.9905	.1059	-2.334	2.2154	1.73×10^{-3}	4.53×10^{-3}
2.0	7.5570	-7.4413	.1389	-2.671	2.8010	9.58×10^{-4}	3.49×10^{-3}
2.2	9.1529	-9.0449	.1669	-3.007	3.4787	5.63×10^{-4}	2.75×10^{-3}
2.4	10.9027	-10.8016	.1910	-3.340	4.2544	3.47×10^{-4}	2.20×10^{-3}
2.6	12.8062	-12.7111	.2118	-3.671	5.1336	2.22×10^{-4}	1.79×10^{-3}
2.8	14.8632	-14.7735	.2301	-4.001	6.1220	1.47×10^{-4}	1.48×10^{-3}
3.0	17.0736	-16.9887	.2462	-4.330	7.2250	1.00×10^{-4}	1.23×10^{-3}
large S	$6S^2/\pi$	$-\overline{\Delta}+\dfrac{1}{\pi S}$	1	$-S\pi/2$	$\dfrac{\sqrt{2}}{4\pi^{3/2}}\,3^{5/4}\,S^{11/4}$	$\pi^2/(15\cdot 3^{5/2}\,S^{11/2})$	$\dfrac{1}{2\pi^2\,S^3}$

Table II

$\mathrm{Re}(\omega R/v_{A_0})$	$-\mathrm{Im}(\omega R/v_{A_0})$	Radial spectrum
0.403	1.26×10^{-2}	18,19 (**18**)
0.411	8.73×10^{-9}	1 (**1**)
0.364	5.53×10^{-3}	15-19 (**17**)
0.379	2.22×10^{-5}	2 (**2**)
0.361	3.93×10^{-4}	3, 4 (**3**)
0.344	1.46×10^{-4}	3-6 (**4**)
0.343	1.53×10^{-3}	3, 4, 6-11, 13-17 (**17**)
0.338	1.70×10^{-3}	4-7, 10-12, 14-18 (**4**)
0.329	1.52×10^{-3}	4-9, 11-13, 15-18 (**5**)
0.320	1.20×10^{-3}	4-7, 9, 10, 12-18 (**6**)
0.311	1.23×10^{-3}	5, 6, 8-11, 12-14, 16-18 (**6**)
0.301	1.65×10^{-3}	4-10, 12, 14-17 (**6**)
0.291	1.84×10^{-3}	6-17 (**7**)
0.281	1.49×10^{-3}	7-13, 15-17 (**8**)
0.271	1.39×10^{-3}	7-12, 14-16 (**9**)
0.260	9.56×10^{-4}	8-11, 15, 16 (**10**)
0.251	7.19×10^{-4}	9-15 (**12**)

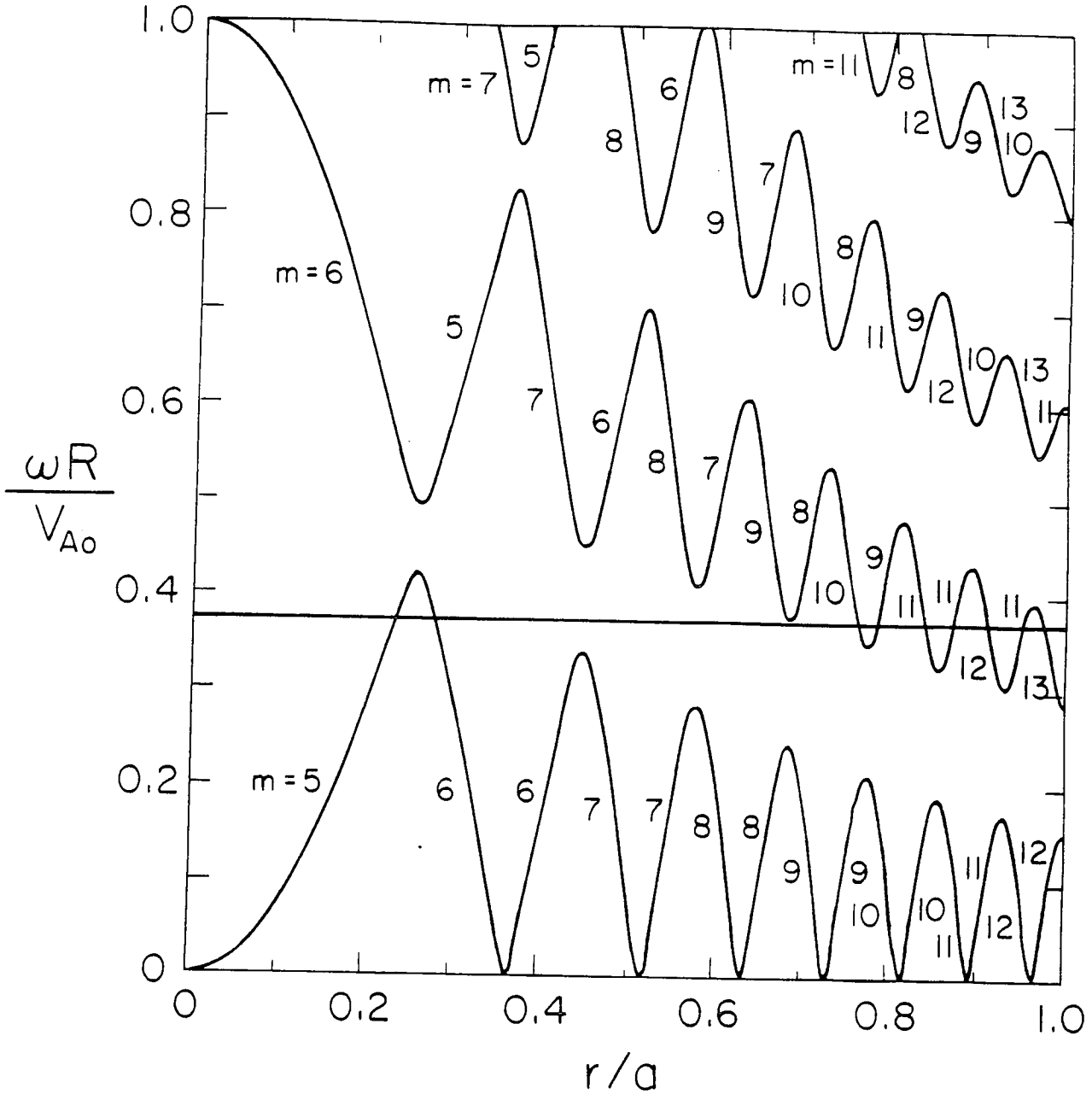

Fig. 1

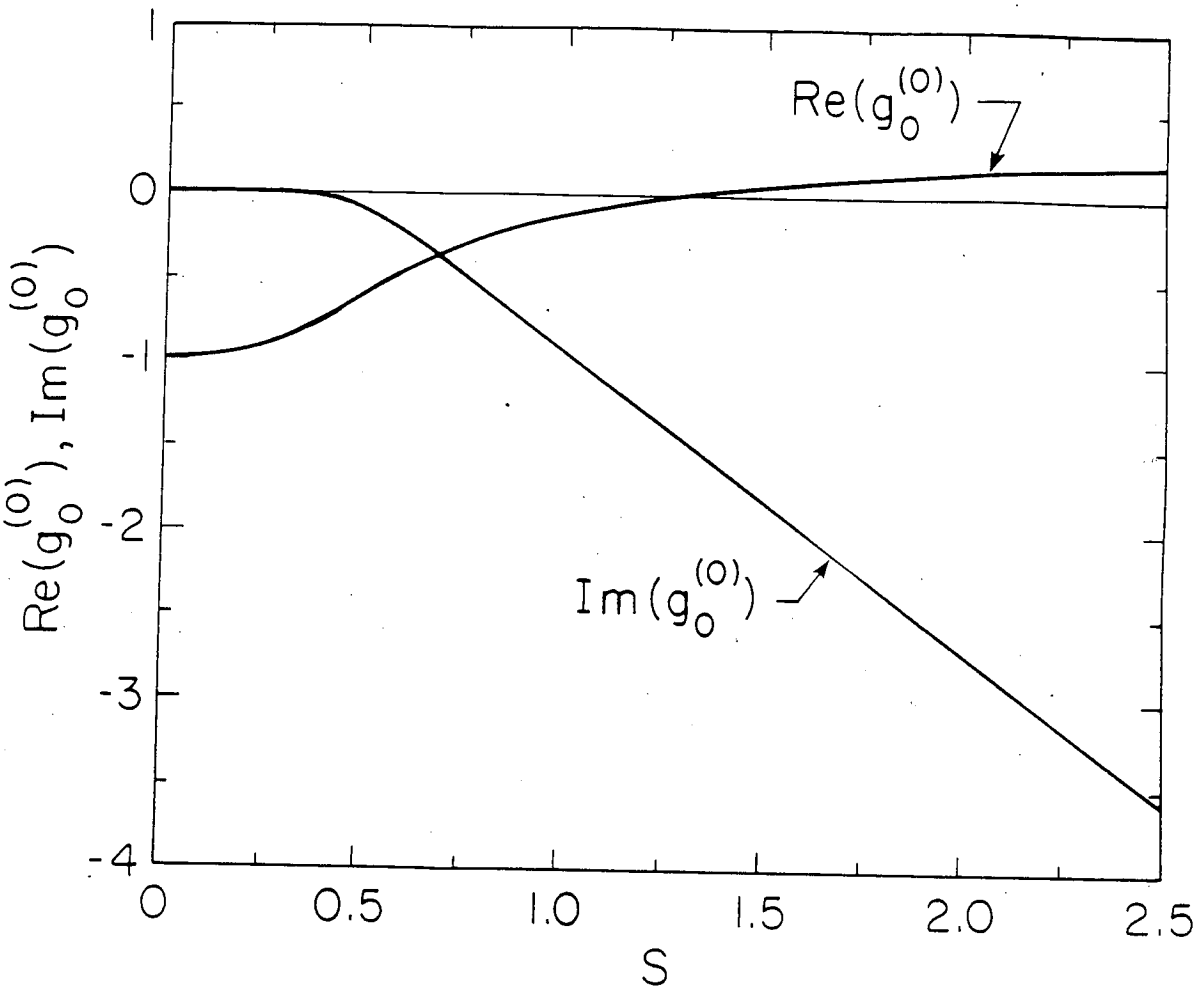

Fig. 2

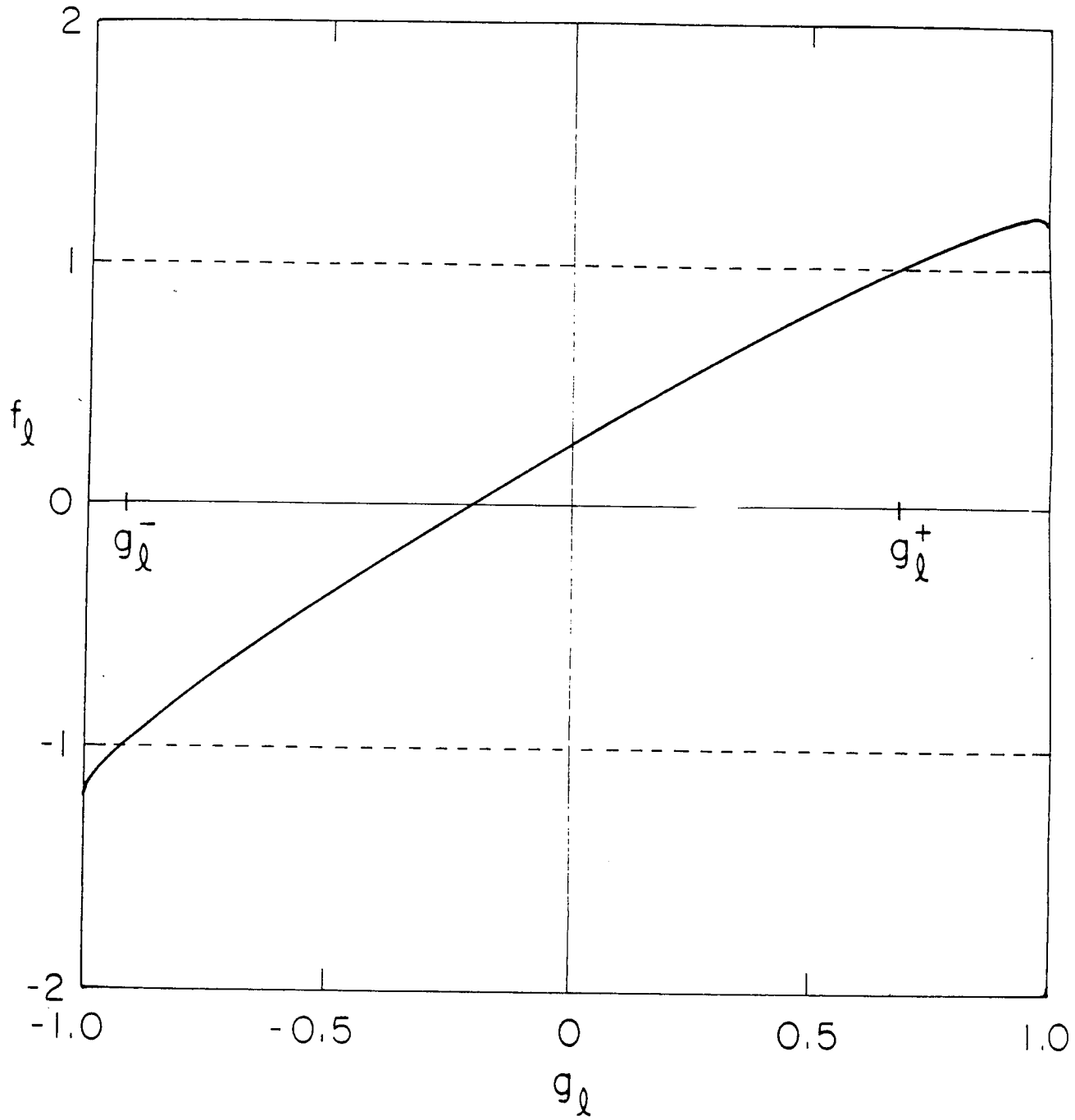

Fig. 3

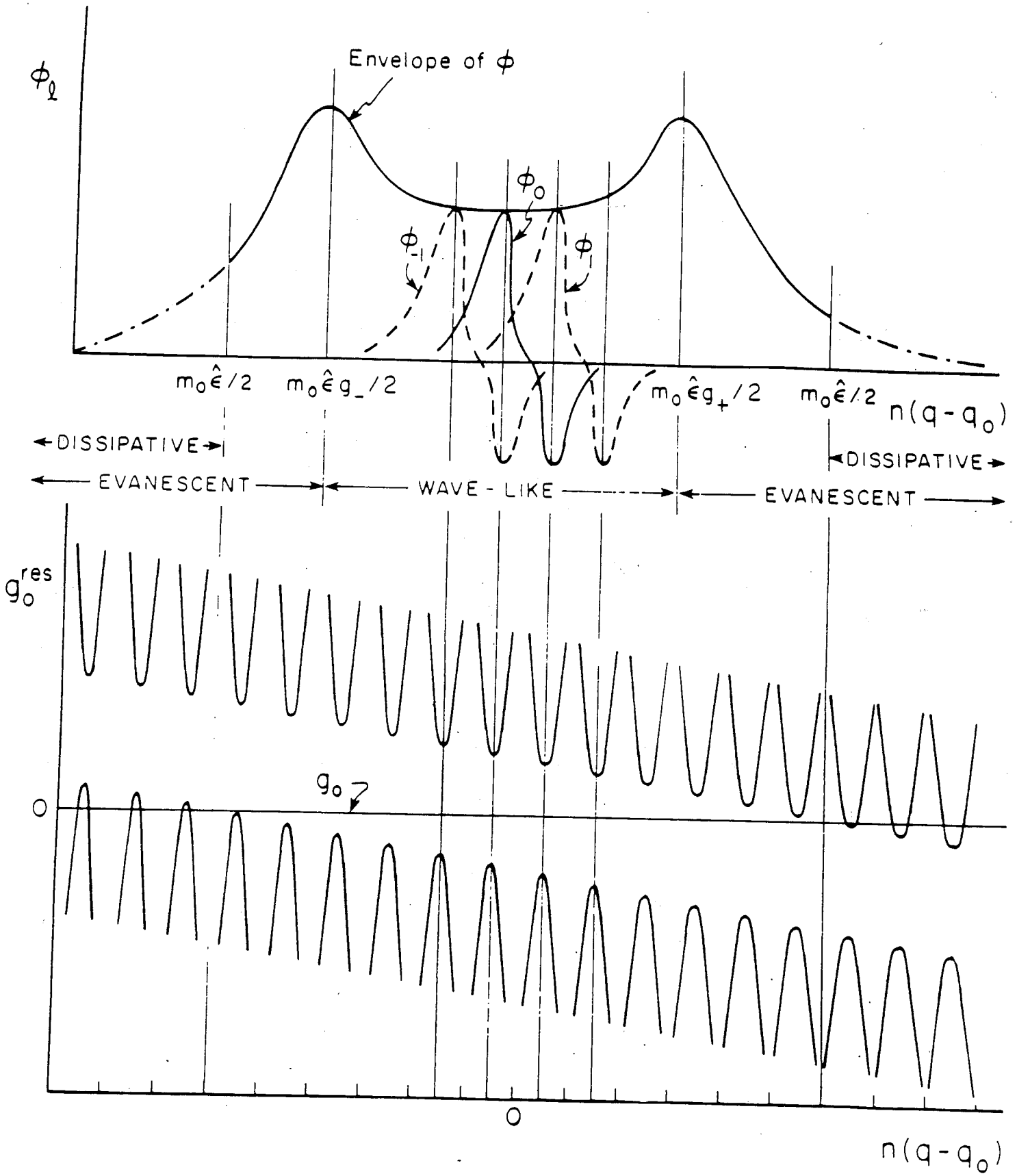
ϕ_ℓ
Envelope of ϕ
ϕ_0
ϕ_{-1}
ϕ_1
$m_0\hat{\epsilon}/2$
$m_0\hat{\epsilon}g_-/2$
$m_0\hat{\epsilon}g_+/2$
$m_0\hat{\epsilon}/2$
$n(q-q_0)$
DISSIPATIVE
EVANESCENT
WAVE-LIKE
EVANESCENT
DISSIPATIVE
g_0^{res}
g_0
0
0
$n(q-q_0)$

Fig. 4

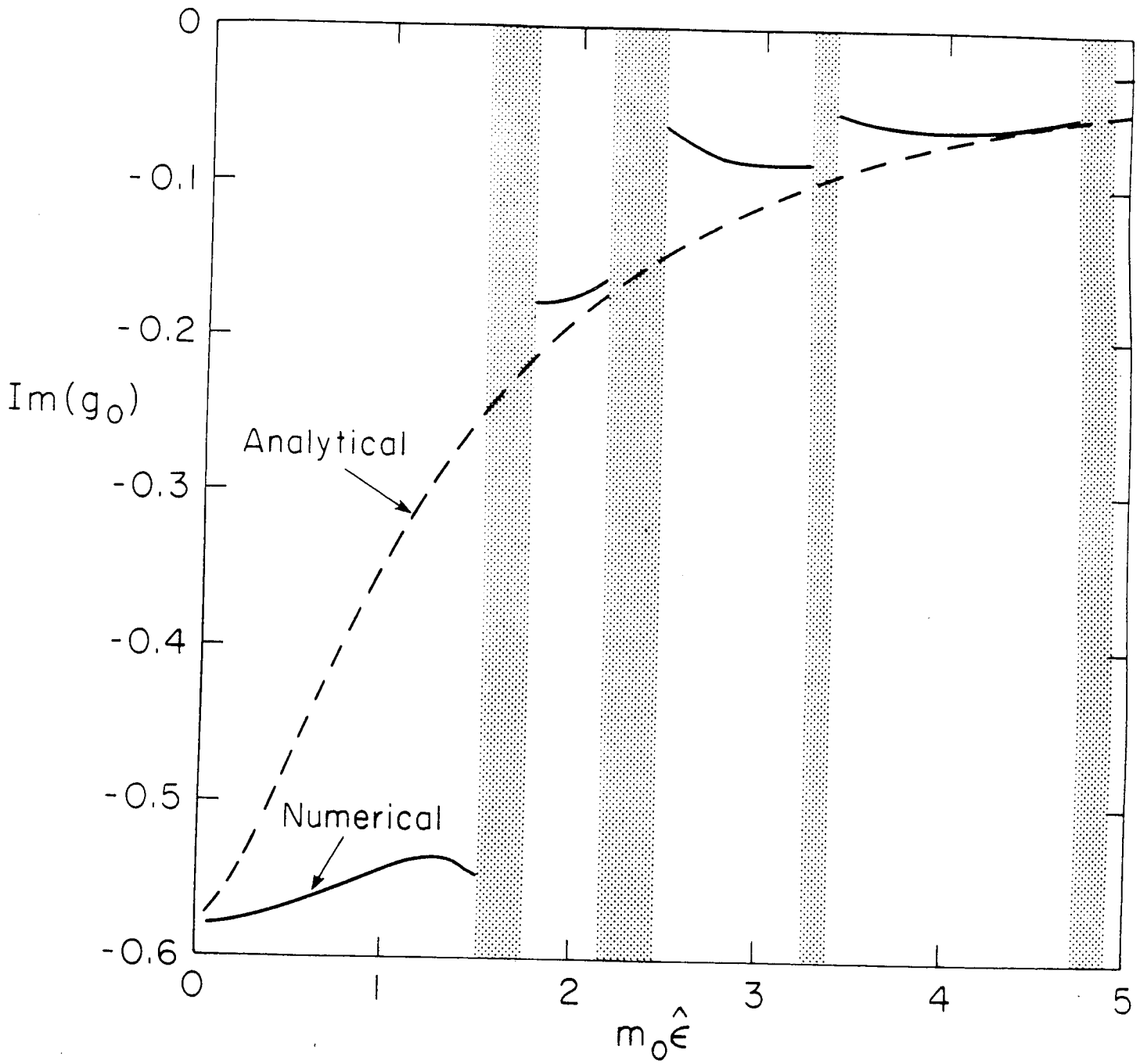

Fig. 5(a)

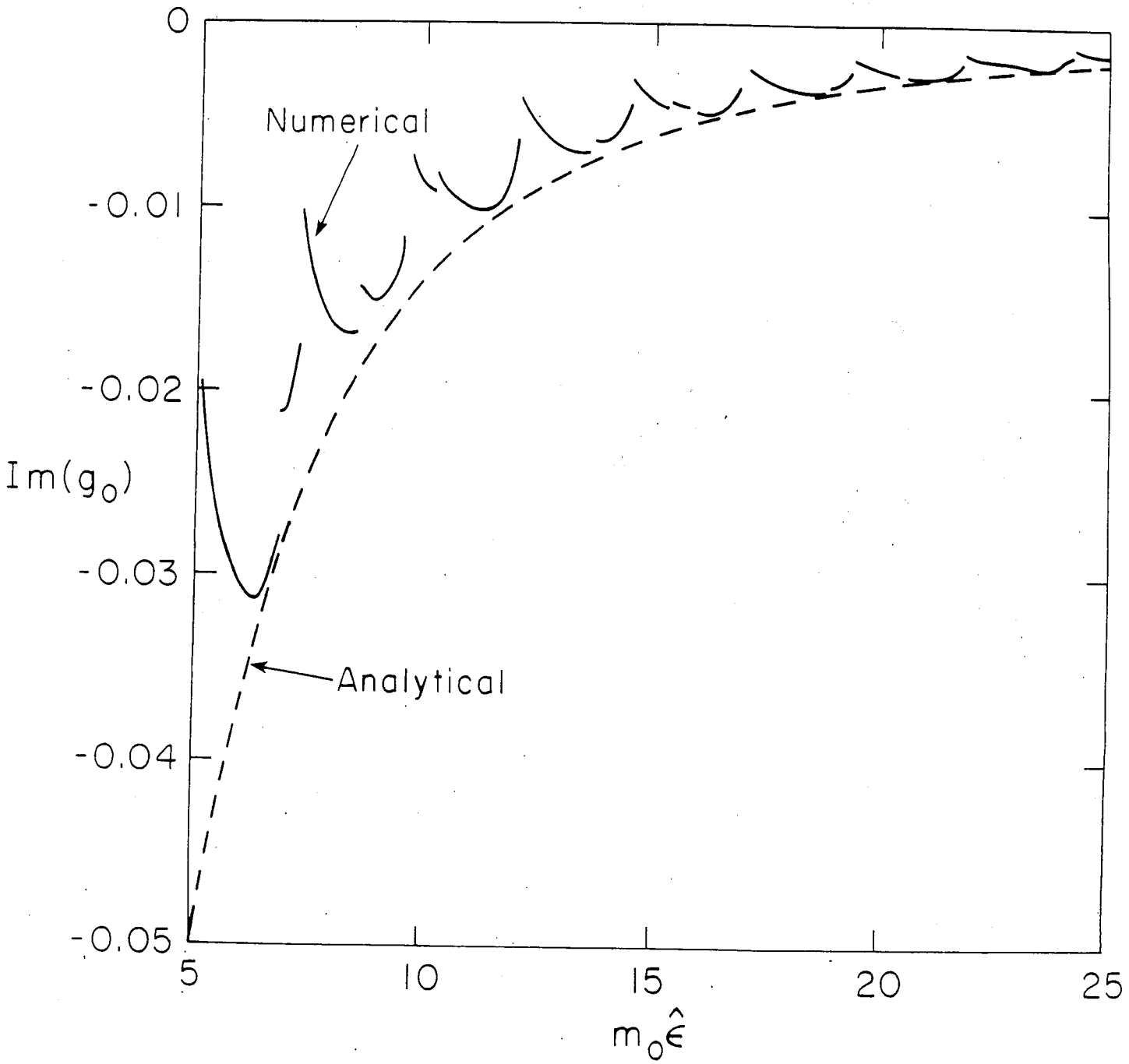
0
-0.01
-0.02
-0.03
-0.04
-0.05
Im(g0)
Numerical
Analytical
5
10
15
20
25
m0ε̂

Fig. 5(b)

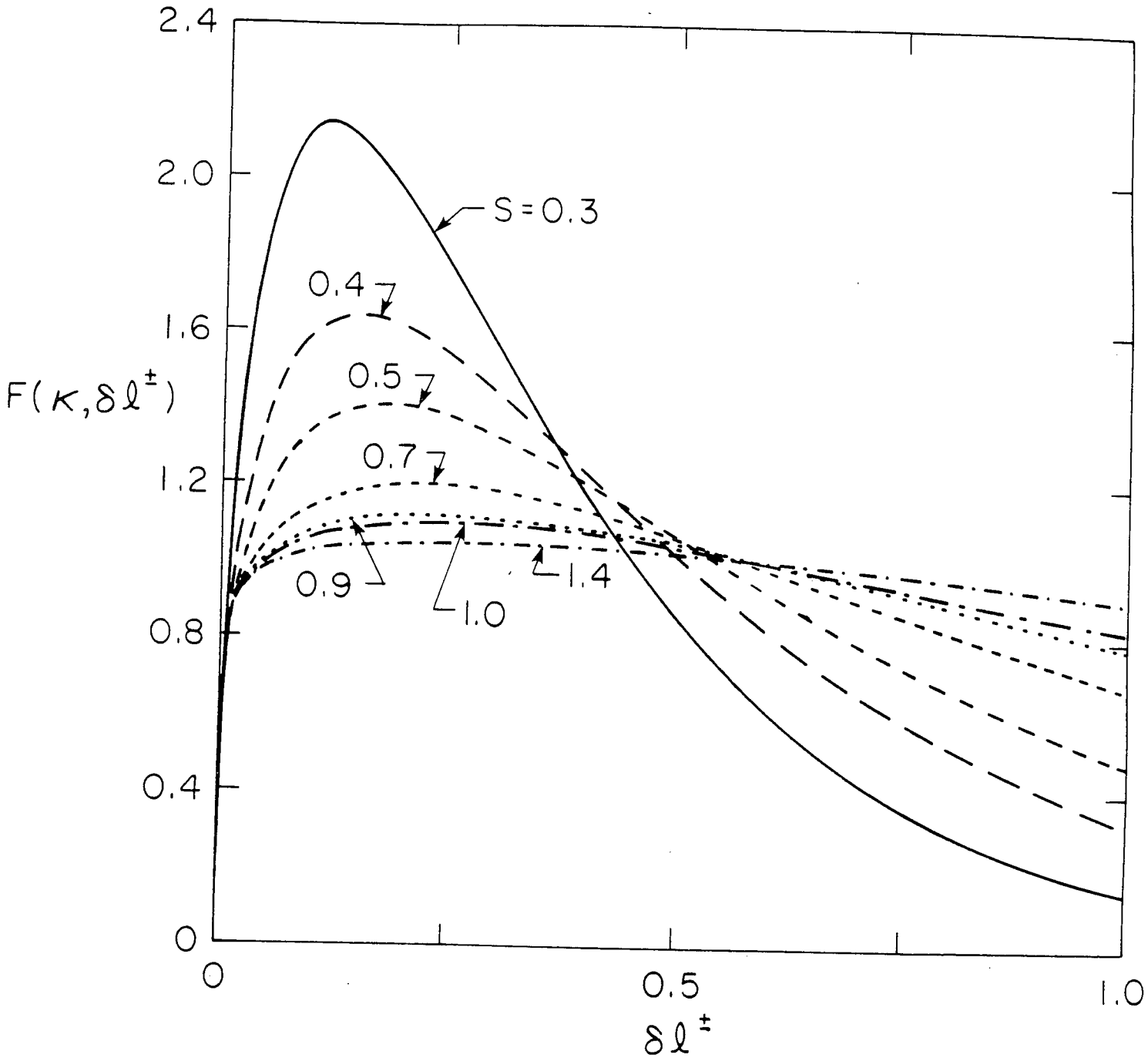

Fig. 6

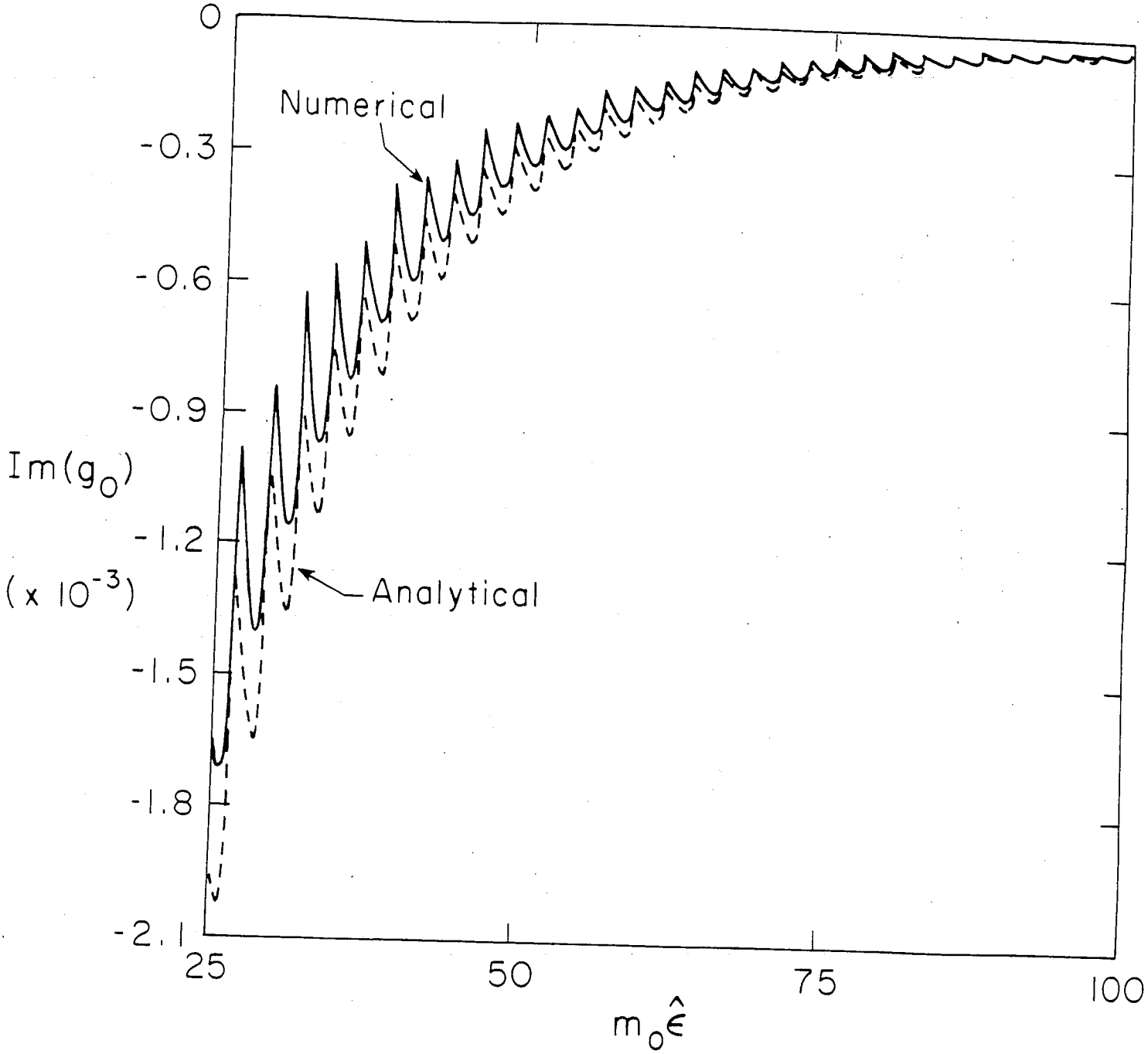
0
-0.3
-0.6
-0.9
-1.2
-1.5
-1.8
-2.1
Numerical
Analytical
Im(g0)
(x 10-3)
25
50
75
100
m0ε̂

Fig. 7

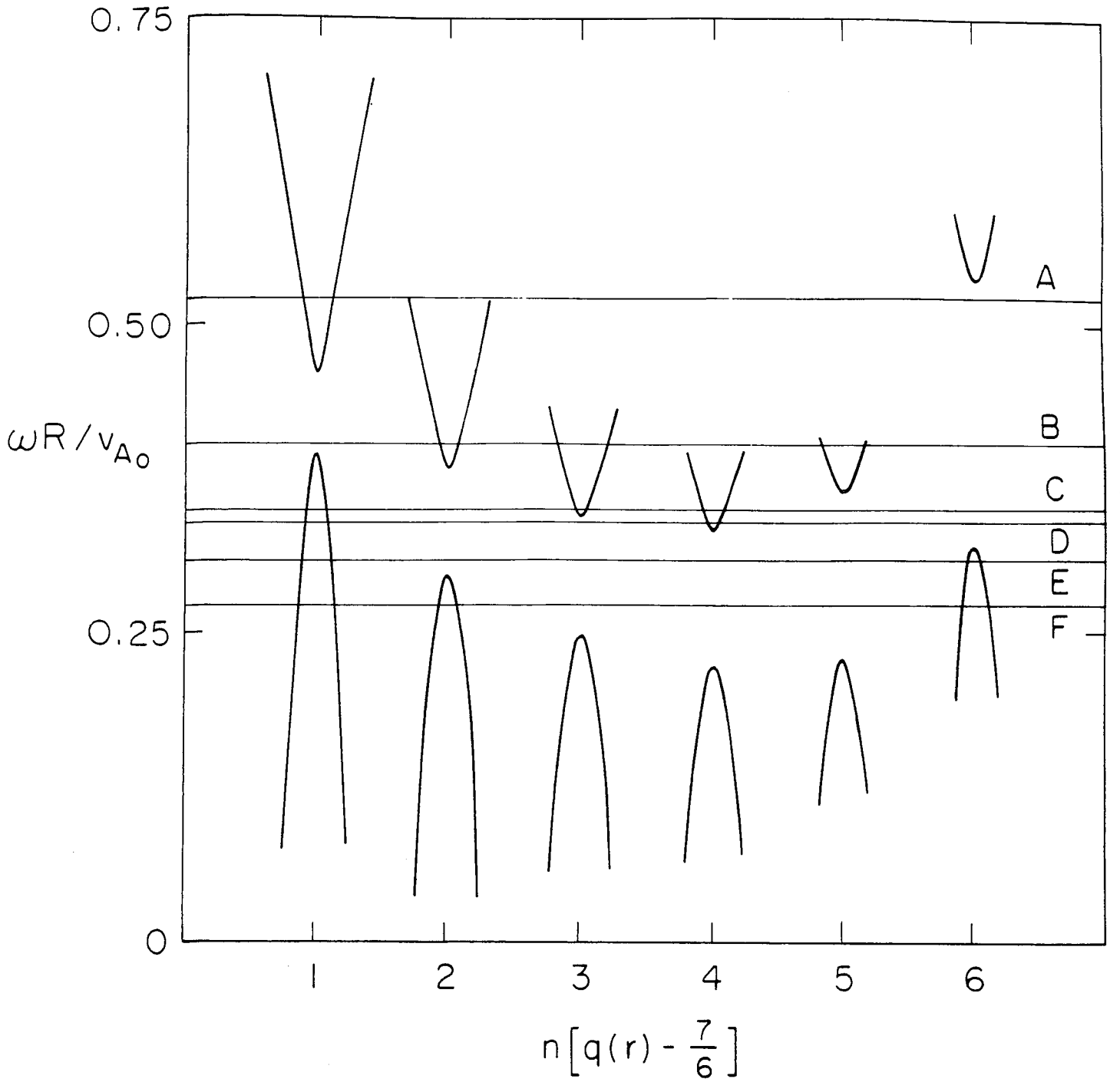

Fig. 8

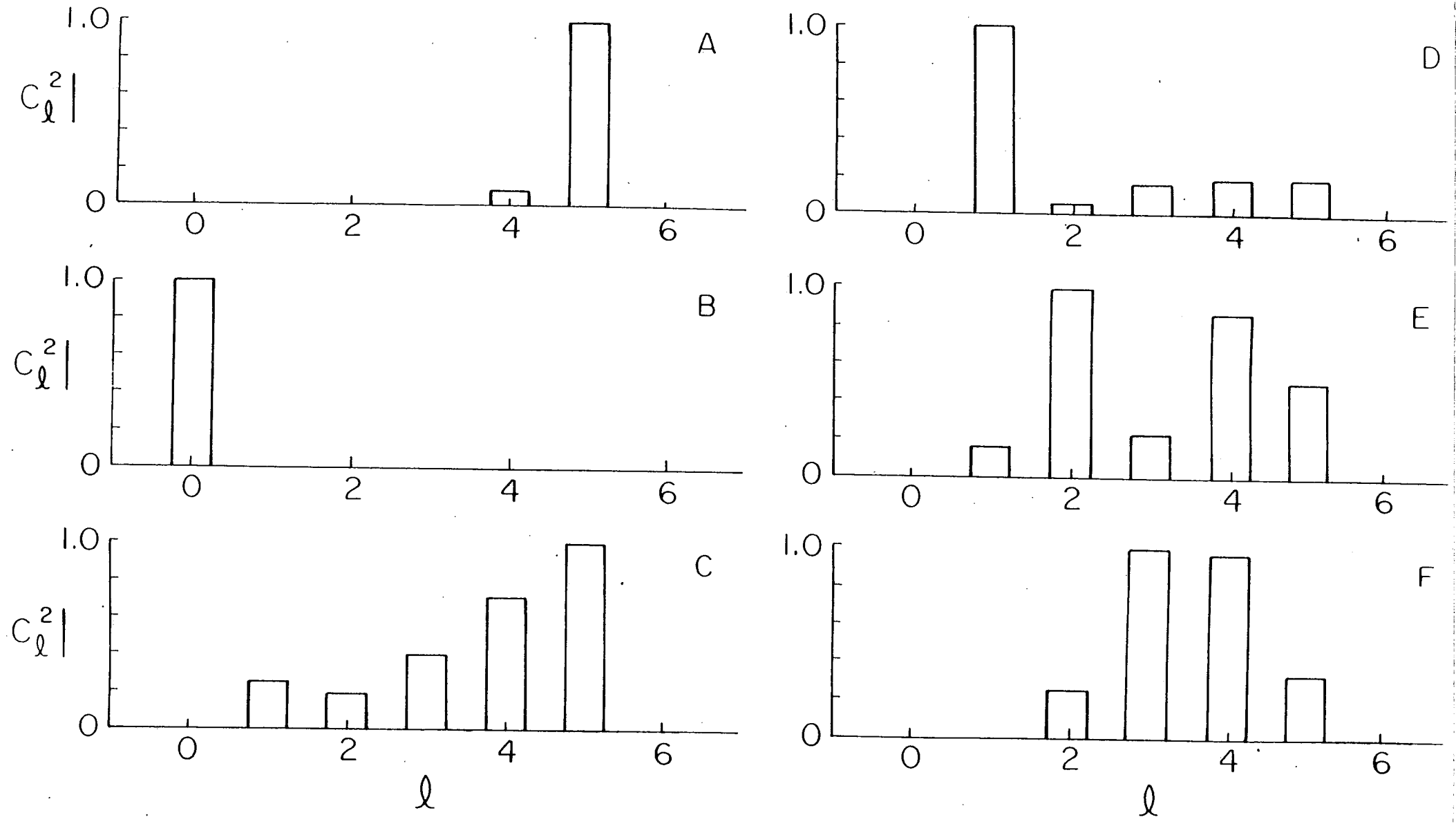

Fig. 9